An efficient multi class Alzheimer detection using hybrid equilibrium optimizer with capsule auto encoder

Published: 14 January 2022

Volume 81, pages 6539–6570, (2022) Cite this article

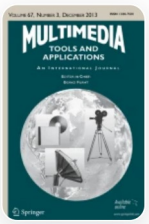

Multimedia Tools and Applications

Aims and scope

Submit manuscript

N. P. Ansingkar, Rita. B. Patil & P. D. Deshmukh

an innovative methodology for the Alzheimer detection in brain image. Initially, an input

image is pre-processed by the skull stripping, and normalized linear smoothing and median joint (NLSMJ) filtering. In the next stage, grey matter (GM), white matter (WM) and cerebrospinal fluid (CSF) brain regions are segmented from the filtered images using adaptive fuzzy based atom search optimizer which is the high convergence rate optimizer for enhancing the segmentation performance. After the image segmentation, GM is registered with the filtered images using the improved affine transformation. Subsequently, features are extracted utilizing improved Zernike features and hybrid wavelet walsh features. Afterwards, features are selected utilizing adaptive rain optimization. Finally, hybrid equilibrium optimizer with capsule auto encoder (HEOCAE) framework is utilized for the detection of Alzheimer, normal and mild cognitive impairment images. The implementation platform used in this work is MATLAB. The presented technique is tested with the ADNI dataset images. The experimental results of the presented technique provide improved performance than the existing techniques in regards of accuracy (98.21%), sensitivity (97.31%), specificity (98.64%), precision (97.45%), NPV (0.098), F1 measure (97.37%) and AUC score (98.29%).

1 Introduction

Alzheimer's disease (AD) is an advanced neurologic disorder that affects persons in numerous cases. The affected individuals are facing difficulties in reading, writing, talking, misperception, and loss of memory [14]. The AD is reflected as the most common cause of age-based dementia. In western cultures, the populace of elder persons are growing day by day and hence, the existence of dementia probable to increase more and more in recent decades. In aged people, AD also cause death. Mild, very mild, and moderate are the three main stages reflected in AD [9]. Still, AD prediction is not provided accurate outcome until a moderate AD is extended by the patient. The earliest identification of AD is an important task to increase potential treatment efficacy. The AD scientific prediction starts with a long preclinical stage, and expansions to mild cognitive impairment (MCI) [12, 21]. CAD (Computer-Aided Diagnosis) schemes are utilized to develop the accuracy for AD prediction complementing the neuropsychological evaluations done by medical specialists [29].

The necessities for AD detection are a complete history of the patient, MMSE (Mini-Mental State Examination), and physical and neurobiological examinations. There are numerous non-invasive neuro imaging tools like PET (Positron Emission Tomography), structural MRI (Magnetic Resonance Image), and functional MRI are deliberated by the many researchers to progress such a system. From all these, MRI is considered by number of researchers because of its features like higher accessibility, better intensity, good contrast, and outstanding spatial resolution [3]. The AD medical check-up always comprises a structural image with MRI or CT (Computed Tomography) [10]. Specially, brain atrophies development was assessed and recognised utilizing biomedical imaging modality and this modality shows a critical role in the brain functionalities assessment [5].

with the high dimensionality voxel-wise features. To state the over fitting issue, feature selection is considered as a major step [8]. Furthermore, the feature selection providing improved classification accuracy depends on the adopted technologies [6]. CNN (Convolutional Neural Network) is one of the most utilized deep learning methodologies and it extensively utilized to identify the healthy brains as well as the Alzheimer's brains [32].

Generally, deep learning approaches providing improved performance in various areas like human action recognition, segmentation of medical images, and visual object recognition [20]. Presently, deep learning dependent CNN has provided outstanding performance in numerous areas, particularly, medical imaging field [30]. The deep learning framework learns the hidden demonstration and capably attains the disease based pathologies for neuro imaging information. Therefore, examiners are in recent times utilizing the deep learning frameworks for the prediction of brain disease as well as AD [28]. Though these approaches are capable, but the substantial challenges remain and pose limitations to the clinical usage.

In AD prediction, the detection of variations in the brain is stabilizes the clinical estimations. Hence, it is deliberated as an important role in the detection of AD at the early stage. Currently, deep learning frameworks are utilized by the various examiners to identify the disease accurately. These deep learning technologies attained improved performances in the analysis of medical image like microscopy, MRI, CT, X-ray, and ultrasound. Therefore, this work presented an improved Alzheimer's disease detection with hybrid equilibrium optimized capsule auto encoder. The major contributions of the presented work is described as,

- To effectively predict the multi class Alzheimer's disease, effective combination of approaches are presented. This enhanced the prediction performance.

- To reduce the feature dimensionality and select the discriminative features using an

adaptive rain optimization methodology.

- Improved image registration process with the grey matter region utilized to attain more detailed information in the feature extraction step.
- To validate the proposed work using standard ADNI dataset and compare it with the recent related research works.

The organization of the research work is described as: Sect. 2 reviews the recent related works, Sect. 3 provides the proposed methodology description in detail, Sect. 4 gives the detailed results and discussion and Sect. 5 concludes the paper.

2 Related work

Manhua Liu et al. [22] had developed a multi-model deep learning structure for joint automatic hippocampal segmentation and AD classification. It was utilized for the convolutional neural network in structural MRI data. At first, a deep CNN framework depends on multi-task was built to learn hippocampal segmentation and categorization of disease. Afterwards, the 3D patches extraction features were done through the construction of 3D densely associated Convolutional Networks (3D DenseNet). At last, the extricated features are combined to classify the disease. The introduced multi modal classification can achieve better performance than the single model approaches. The developed approach provides the better performance in AD prediction. However, the performance on accuracy can be improved further.

Katia M. Poloniet al. [26] presented a newest methodology to perform MR image classification

approaches. Moreover, other recent modalities can be used for further improvement.

Jinwang Feng et al. [11] proposed an innovative methodology to attain correlations of the abnormal energy distribution patterns connected to AD through assembling non subsampled contourlet sub band-based individual networks (NCSINs) in the domain of frequency. A 2-dimensional demonstration of the pre-processed sMRI image was initially redesigned through down sampling and recreation procedures. Afterwards, the non-subsampled contourlet transform was accomplished on the 2Ddemonstration to attain guiding sub bands. Every directional sub band at the scale was designated through a column energy feature vector (CV) observed as a node of the NCSIN. Next, edge amongst any two nodes was weighted with connection strength (CS). At the end, the concatenation of node and edge features of the NCSINs at differing scale was utilized as a network feature of the sMRI image for better AD classification. However, the performance of the developed approach was not enhanced in different performance metrics. The performance can be improved by using the deep learning approaches.

Nawaz et al. [24] presented a smart and accurate methodology of identifying AD depends on a two-dimensional deep CNN (2D-DCNN) through an imbalanced 3D MRI database. The model classifies MRI into three different classes are AD, MCI and CN. The developed methodology was depends on the DCNN framework. Moreover, the framework was considered for predicting the categories of MRI as AD, MCI and CN. Hence, it was supporting the multiple class of classification utilizing the CNN framework. Moreover, the multiple classifications accurately predict the AD at the earliest stage. But still, better validation can be provided to validate the results.

Riyaj Uddin Khan et al. [18] had presented an innovative methodology to classify MCI, normal

accuracy from the attained features. The developed approach used the machine learning approach for processing. The deep learning approach can be further used for improving the classification approach performance.

Kruthika et al. [19] developed a 3D capsule network (CapsNets), 3D auto encoder and convolutional neural network for the early prediction of Alzheimer's disease. The CapsNets was utilized for predicting the AD fast through deep learning. The ensemble classifier approach was presented in this work accurate prediction of AD disease effectively. The developed combination of approach provides the robust performance in the classification of AD diseased images. Further, the performance on AD prediction can be improved by increasing the number of layers.

Tooba Altaf et al. [2] introduced an effective classification of AD disease by utilizing the hybridized features. Here, the GLCM (grey level co-occurrence matrix) feature extraction approach was utilized for extracting the features effectively. Moreover, the clinical features were utilized for enhancing the accuracy in AD prediction. The hybrid features were enhancing the performance on AD prediction. Performance can be enhanced by using different performance metrics.

Kongtao Chen et al. [7] presented a structured pruning framework of convolutional networks on tensor processing unit. Here, VGG-16 model was utilized for accurately predicting the Alzheimer's disease. The structure pruning framework was a capable approach for predicting the AD disease and its stages. This framework was utilized to enhance the performance of deep learning technique on tensor processing units.

Atif Mehmood et al. [23] introduced a Siamese convolutional neural network (SCNN)

Mehreen Ahmed et al. [1] investigated a various neuro imaging and machine learning based

approaches in AD prediction. Especially, ensemble approaches were providing higher accuracy than the other general approaches. The large amount of database with different stages of AD providing better prediction with the machine and deep learning approaches. However, the performance on various metrics can be improved by the better feature extraction and classification methodologies.

In the existing works, different machine learning approaches are presented for the Alzheimer's detection. The approaches are not validated for various performance metrics to analyse the performance of the presented approach. The presented approach using the hybrid deep learning approach for accurate prediction of the Alzheimer's classes. Moreover, the performance of the approach is enhanced by the effective combination approaches used in pre-processing, feature extraction and feature selection. The presented approach considered the standard ADNI dataset images for the Alzheimer detection with the hybrid deep learning approaches. Moreover, the performance of the presented approach is validated by comparing different recent existing approaches with the different performance metrics.

3 Proposed methodology

This paper presented Alzheimer detection in the brain image utilizing hybrid optimized capsule auto encoder framework. Initially, an image is pre-processed by the back ground exclusion with double threshold (DT) based skull stripping and NLSMJ filtering. After the removal of noises in the images grey matter (GM), white matter (WM) and cerebrospinal fluid (CSF) regions are segmented from the pre-processed images with fuzzy based atom search optimizer which is the high convergence rate optimizer for enhancing the segmentation accuracy. Subsequently, the segmented GM is registered with the pre-processed image using

Fig. 1

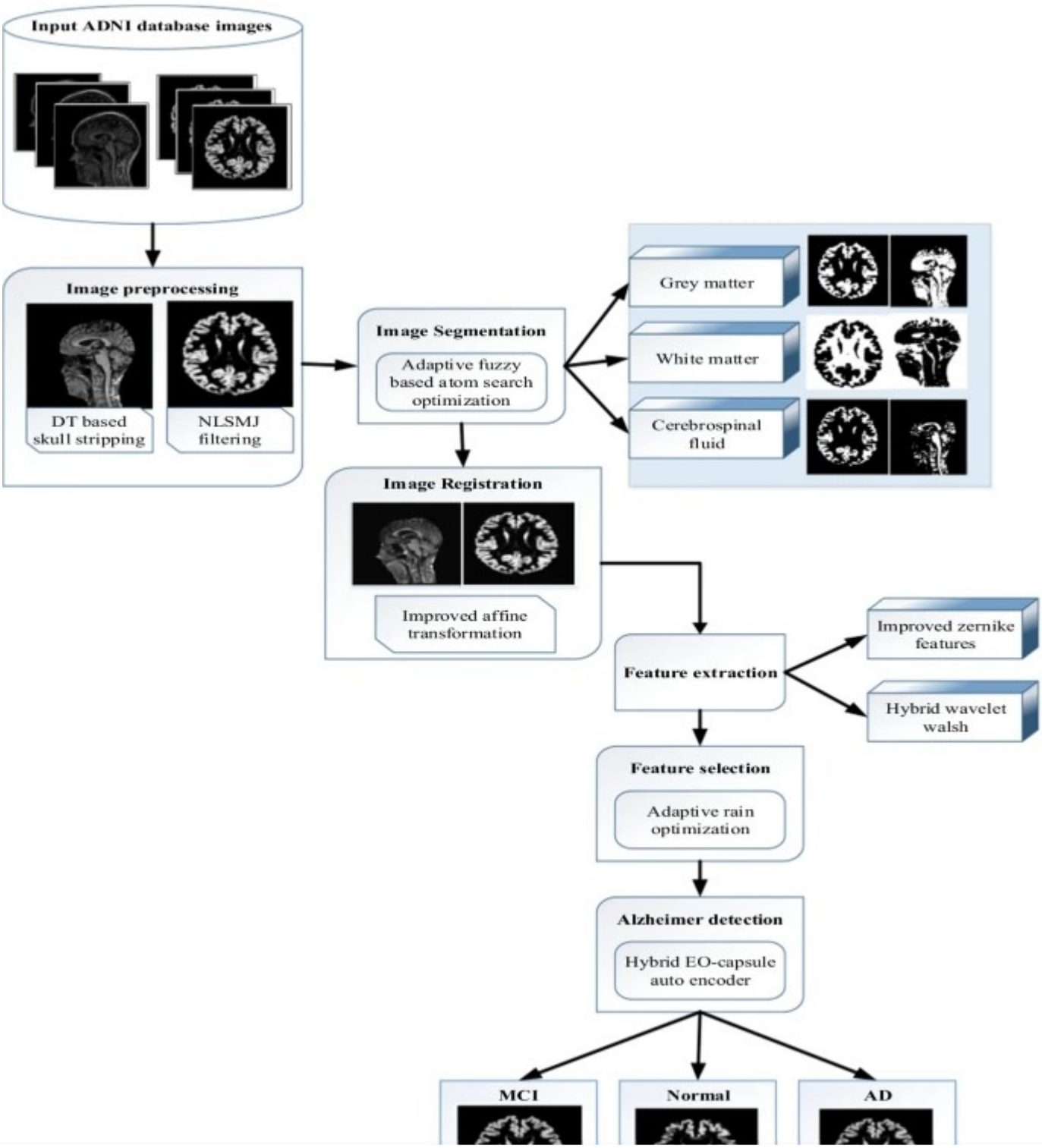

Initially, the input images are pre-processed with DT based skull stripping and NLSMJ based filtering for enhancing the ADNI dataset images. The image pre-processing procedures are described in subsequent sections,

3.1.1 DT based skull stripping

In the presented approach, the skull is stripped with the double threshold (DT) based process. Here, double threshold values are utilized for differentiating the intensities of the skull regions in the image. The range is taken as 0 to 0.5 and 0.7 to 1. Then the higher intensity range regions are removed from the image. The higher intensity regions are the skull regions in the image. The skull region is generally brighter than the other regions. The DT based skull stripping is attained through the condition (1),

$$I\left(y,z\right)=\left\{\begin{array}{l}1\kern0.72em for\kern0.48em 0.2\le {D}_T\le 0.7\\{}0\kern0.72em else\end{array}\right.$$

(1)

Here, $I(y, z)$ represents the skull stripped image and D_T represents the double threshold. Here, the skull region is above 0.7 range.

3.1.2 Normalized linear smoothing and median joint (NLSMJ) filtering

The Min-Max normalization is applied to fit the image in fixed dimension utilizing the condition (2). So that the image acquired at different condition have same characteristics.

$${\bar{N}}_I(z)=\frac{A-{A}_{\min }}{A_{\max }-{A}_{\min }}$$

smoothing filtering is described through the subsequent condition (3),

$$\bar{F}\left(y,z\right)=\frac{1}{cd}\sum \limits_{\left(u,v\right)\in {R}_{y,z}} g\left(u,v\right)$$

(3)

Here, $R_{y,z}$ signifies the set of coordinates in the rectangular sub image window, the pixels at the middle is represented as (y,z) and the noisy image is denoted as $g(u,v)$. This filtering is combined with the median filtering to jointly enhance image. The linear smoothing filtering process improves the intensity variation and at the same time median filtering preserves the edge details in the image without decreasing quality of the image. Moreover, this filtering process effectively eliminates the salt and pepper noises in the image. The median filtering is computed through the condition (4),

$$\bar{F}\left(y,z\right)={Md}_{\left(s,t\right)\in Kyz}\left\{g\left(s,t\right)\right\}$$

(4)

Here,K_{yz} represents the set of coordinates at a point centred (y,z).The major aim of filtering an image is to eliminate the noises on the digital images. The quality of the image is decreased by the noises. To enhance the image by removing the noises present in the image is filtering process. Here, normalized bilateral filtering is utilized to enhance the images.

3.2 Image segmentation using adaptive fuzzy clustering based atom search optimization

(5)

Afterwards, the membership function matrix \({M}^{(p)}=\left\{{m}_{st}^{(p)}\right\}\) is attained through the individual membership functions through the subsequent condition (6),

$${m}_{st}^{(p)}=\frac{1}{\sum \limits_{p=1}^k{\left(\frac{\left\Vert {y}_s-{q}_t^{(p)}\right\Vert }{\left\Vert {y}_s-{q}_k^{(p)}\right\Vert}\right)}^{{~}^{2}\!\left/ \!{~}_{k-1}\right.}}$$

(6)

Here, $\|\cdot\|$ represents the norm stating the difference or the Euclidean distance between the perceived data and the centre, k represents the index of the fuzziness coefficient range from 1 to infinity. The centroid \({C}_k^{\left(p+1\right)}\) at $(p+1)^{th}$ step is updated through the condition (7),

$${C}_t^{\left(p+1\right)}=\frac{\sum_{s=1}^n{m}_{st}^{\left(p+1\right)k}{y}_t}{\sum_{s=1}^n{m}_{st}^{\left(p+1\right)k}}$$

(7)

Here, the position of the centroid is updated through the atom search optimization procedure. The location of clustering pixels are updated through the condition (8),

$${Z}_k\left({t}^{\prime }+1\right)={Z}_k\left({t}^{\prime}\right)+{\bar{V}}_k\left({t}^{\prime }+1\right)$$

(8)

^{\prime}\right)+{a}_k\left({t}^{\prime}\right)$$

(9)

Here, \(\hat{J}\left(C,M\right)\) signifies the initially attained clustering outcomes and $a_k(t^{'})$ represents the acceleration of the k^{th} atom in the $t^{'}$ iteration and it is attained through the condition (10),

$${a}_k\left({t}^{\prime}\right)=-\bar{\eta}\left({t}^{\prime}\right)\sum \limits_{k\in Nbest}\frac{\hat{R}\left[2\ast {\left({q}_{pk}\left({t}^{\prime}\right)\right)}^{13}-{\left({q}_{pk}\left({t}^{\prime}\right)\right)}^7\right]}{D_p\left({t}^{\prime}\right)}\times \frac{z_p\left({t}^{\prime}\right)-{z}_k\left({t}^{\prime}\right)}{z_p\left({t}^{\prime}\right)\ast {z}_k\left({t}^{\prime}\right)}+\overset{\frown }{\beta }{e}^{\frac{-20{I}_{\max }}{I_{\max }}}\frac{z_{best}\left({t}^{\prime}\right)-{z}_p\left({t}^{\prime}\right)}{D_p\left({t}^{\prime}\right)}$$

(10)

Here, *Nbest* represents the best atoms set, z_{best} represents the best atom in the current location, \(\overset{\frown }{\beta }\) represents the weights of the multiplier and \(\bar{\eta}\left({t}^{\prime}\right)\), $q_{pk}(t^{'})$, $D_p(t^{'})$ functions are evaluated with the subsequent conditions are described as,

$$\bar{\eta}\left({t}^{\prime}\right)={\alpha}_w\ast {\left(1-\frac{1-1}{I_{\max }}\right)}^3\ast {e}^{\frac{-20{I}_{\max }}{{\mathrm{I}}_{\max }}}$$

(11)

\frac{d_{pk}\left({t}^{\prime}\right)}{\sigma \left({t}^{\prime}\right)}>{q}_{\max

}\kern1.08em \end{array}\right.$$

(12)

$${d}_p\left({t}^{\prime}\right)=\frac{D_p\left({t}^{\prime}\right)}{\sum \limits_{k=1}^{\bar{N}}{D}_k\left({t}^{\prime}\right)}$$

(13)

Here, α_w denotes the depth weight, $I_{\max}$ represents the maximum number of iterations and $d_{pk}(t^{'})$ represents the distance among p^{th} and k^{th} atoms at the $t^{'th}$ iteration. Moreover, the variables $q_{\min}$, $q_{\max}$, $\sigma(t^{'})$ and $D_p(t^{'})$ are evaluated through the subsequent conditions as,

$${q}_{\min }={\bar{g}}_0+\bar{g}\left({t}^{\prime}\right)\kern0.5em \&\kern0.5em {q}_{\max }=\bar{u}$$

(14)

$$\sigma \left({t}^{\prime}\right)={z}_{pk}\left({t}^{\prime}\right),\frac{\sum \limits_{k\in Nbest}{z}_{pk}\left({t}^{\prime}\right)}{k\left({I}_{\max }\right)}$$

(15)

The clustering iterations reduces the errors through the subsequent fitness condition (16),

$$\hat{J}\left(C,M\right)=\sum \limits_{s=1}^n\sum \limits_{t=1}^k{m}_{st}^k{\left\Vert {y}_s-{q}_t\right\Vert}^2$$

$${D}_p\left({t}^{\prime}\right)={e}^{-\frac{Fitness_k(t)-{Fitness}_{best}(t)}{Fitness_{worst}(t)-{Fitness}_{best}(t)}}$$

(17)

The process is repeated until the maximum iteration reaching the satisfying solution with the condition of $\|D^{k+1}{}_p(t^{'})) - D^{k}{}_p(t^{'})\| < \epsilon$. The proposed atom search optimized fuzzy clustering effectively segments the regions of white matter, grey matter and the cerebrospinal fluid in the images.

3.3 Image registration using improved affine transformation

In the presented work, the segmented grey matter regions are registered on the filtered images. The operations like translation, scaling and rotations are considered as an affine transformation. This conserves the operations of linearity among the points and the distance ratios among the line. This clears that any point can be a collinear before the transformation operation and the same point remains same after the transformation process. The process of image registration using the affine transformation is coherent mapping among the source and the target image. Here, the segmented grey matter is mapped into the pre-processed input image. The improved affine transformation is described in the subsequent condition (18),

$$\left[\begin{array}{l}{y}^{\prime}\\ {}{z}^{\prime}\end{array}\right]=\left[\begin{array}{l}P\kern1.2em Q\\ {}R\kern1.32em S\end{array}\right]\left[\begin{array}{l}y\\ {}z\end{array}\right]+\left[\begin{array}{l}C\\ {}D\end{array}\right]$$

(18)

In this section, improved Zernike features and hybrid wavelet and walsh features are extracted from the registered images. The appropriate feature extraction process helps in the effective differentiation of Alzheimer diseased images.

3.4.1 Improved Zernike features

The improved Zernike features in the order of k with the replication of p are attained through the condition (19),

$${Z}_{kp}=\frac{k+1}{\pi}\sum \limits_y\sum \limits_z{f}^{\prime}\left(y,z\right)\;{U}_{kp}\left(y,z\right),\kern0.84em {y}^2+{z}^2\le 1$$

(19)

Here, the Zernike features Z_{kp} on swapped image having similar magnitudes. Consequently, $|Z_{kp}|$ represents the features rotational differences, $U_{kp}(y, z)$ signifies a polynomial of Zernike in the unit circle $y^2 + z^2 \leq 1$. The polynomial of Zernike feature is evaluated through the condition (20),

$${U}_{kp}\left(y,z\right)={U}_{kp}\left({\rho}^{\prime },{\theta}^{\prime}\right)={Q}_{kp}\left({\rho}^{\prime}\right)\exp \left(ip{\theta}^{\prime}\right)$$

(20)

Here,

$${Q}_{kp}\left({\rho}^{\prime}\right)=\sum \limits_{t=0}^{\frac{k-\left|p\right|}{2}}

^{-1}\frac{y}{z}\).

3.4.2 Hybrid wavelet feature and Walsh transform

The hybridized wavelet and Walsh features are extracted in this section for the accurate differentiation of images. The feature utilizes the dynamic scales and positions of the wavelet for the representation. Consider function of square integral as $z(t)$ and the continuous wavelet transform of the $z(t)$ to a given wavelet $\psi(t)$ is described as,

$${\bar{W}}_{\psi}\left(c,d\right)=\int_{-\infty}^{+\infty }z(t){\psi}_{c,d}(t) dt$$

(22)

$${\psi}_{c,d}(t)=\frac{1}{\sqrt{c}}\psi \left(\frac{t-c}{d}\right)$$

(23)

Here, the wavelet $\psi_{c,d}(t)$ is evaluated from the mother wavelet $\psi(t)$ through transformation and dilation operations, c denotes the dilation factor and d denotes the translation factor. Here, Haar wavelet function is considered due to its usage in various applications. The condition (22) is discretized through limiting the c and d components into a discretized lattice ($c = 2^b$ & $c > 0$) to provide an discretized wavelets and they are described in the subsequent conditions (24) and (25),

$${\bar{CG}}_{l,m}(n)=\downarrow \left[\sum \limits_nz(n){\bar{L}}_l^{\ast}\left(n-{2}^lm\right)\right]$$

(24)

pass and high pass filter correspondingly, l, m signifies the scale of the wavelet and translation

factors, ↓ represents the operation of down sampling. The walsh transform of the data samples of $z(n)$ and $n = 1, 2, 3...N'$ is described in the condition (26),

$${Z}_w(p)=\sum \limits_{n=1}^{N^{\prime }}z(n){\bar{Wa}}_n\kern0.36em p=1,2,3.\dots \bar{N}$$

(26)

Here, $\bar{N}$ represents the number of pixels in the image, ${\bar{Wa}}_n$ represents the Walsh function and it is described through the condition (27),

$${\bar{Wa}}_n=\frac{1}{2^{{~}^{n}\!\left/ \!\![~]_{2}\right.}}\left(\begin{array}{l} {\bar{Wa}}_{n-1}\kern1.2em {\bar{Wa}}_{n-1}\\ {}{\bar{Wa}}_{n-1}\kern0.96em -{\bar{Wa}}_{n-1}\end{array}\right)$$

(27)

In 1 × 1 considered matrix, value of the ${\bar{Wa}}_o$ value is equivalent to 1. Hence, ${\bar{Wa}}_1$ and ${\bar{Wa}}_2$ are described as,

$${\bar{Wa}}_1=\frac{1}{\sqrt{2}}\left[\begin{array}{l}1\kern1.32em 1\\ {}1\kern0.84em -1\end{array}\right]$$

(28)

$${\bar{Wa}}_2=\frac{1}{2}\left[\begin{array}{l}1\kern1.32em 1\kern1.08em 1\kern1.08em

$${\bar{Wa}}_n=\prod \limits_{k=1}^{n}\left(-1\right)^{n_k{L}_{n-k}}$$

(30)

The walsh transform is a multiplication of data sequence with length 1 × N and the Walsh matrix with length of N × N. Finally the hybrid wavelet and the walsh transform is attained through the product of wavelet and walsh functions with the condition (31) described as,

$${F}_{hybrid}={\bar{CG}}_{l,m}(n)\times {\bar{CD}}_{l,m}(n)\times {\bar{Wa}}_n$$

(31)

Here, F_{hybrid} represents the hybrid wavelet and walsh feature, \({\bar{CG}}_{l,m}(n)\) represents the gross components of the wavetet, \({\bar{CD}}_{l,m}(n)\) denotes the detailed components in the wavelet and \({\bar{Wa}}_n\) represents the walsh function.

3.5 Feature selection with adaptive rain optimization

The rain optimization algorithm follows the falling of rain drop behaviour from the higher position to the lower position. The proposed rain optimization initially starts with the population of extracted features. Consider the size of the population as \(\bar{Y}\), the number of drops is described in the condition (32),

$${N}_d=\left[{\bar{V}}_{n,1},{\bar{V}}_{n,2},{\bar{V}}_{n,3}.\dots {\bar{V}}_{n,m}\right]$$

(32)

condition (34),

$${\bar{V}}_{n,m}={D}_u\left({\bar{U}}_m,{\bar{L}}_m\right)$$

(34)

Here, D_u represents the uniform distribution function, \({\bar{U}}_m\) and \({\bar{L}}_m\) represents the upper and lower limits of m. The position of the optimization variables neighbourhood (N) are considered arbitrarily through the condition (35),

$$\left\Vert \left({N}_d-{N}_p\right)\cdot {\bar{V}}_m\right\Vert \le \left\Vert {\bar{R}}_p\cdot {\bar{V}}_m\right\Vert .$$

(35)

$${\bar{R}}_p={\bar{R}}_p\left(Initial\ast Iteration\right)$$

(36)

Here, \({\bar{R}}_p\) signifies the real positive number denoting neighbour point N_p, $(\cdot)$ operator represents the m^{th} size unit vector. In all the neighbourhood points dominant point is considered for the optimal feature selection through the condition (37),

$${F}_O\left({DN_p}_n^m\right)<{F}_O\left({N_p}^m\right)$$

(37)

$${F}_O\left({DN_p}_n^m\right)<{F}_O\left({N_p}_n^m\right)\kern0.84em n\in \left\{1,2,3,\dots {N}_p\right\}$$

$${N}_p(Optimal)={N}_p\ast {R}_B\ast {R}_C$$

(39)

Here, $N_p(Optimal)$ represents the neighbouring point number in the optimal condition with no eruption, R_B represents the base of removing data and R_C represents the removing data count.

The optimal ranking of features using the optimization is computed through the subsequent condition (40),

$${F}_{rank}= order\left({OF}_1\right)\ast order\left({OF}_2\right)$$

(40)

Here,

$${\bar{OF}}_1={F}_O\left|{I}_{\max }-{F}_O\right|\kern0.48em at\kern0.36em {1}^{st}\; iteration$$

(41)

$${\bar{OF}}_2={F}_O\kern0.48em at\kern0.24em {N}^{th}\; iteration$$

(42)

Here, $I_{\max}$ represents the maximum iteration, OF_1 and OF_2 represents the changes occurs in the objective function from the 1^{st} iteration to the N^{th} iteration. From the condition (40), the

TheHybrid Equilibrium Optimizer with Capsule Auto Encoder is utilized for the classification

of Alzheimer's disease into normal, MCI and AD. The hybrid capsule Auto encoder function (\(\bar{F}\)) mapping the input (y) to representation (h) and the decoder mapping the representation h into the y output. The encoder encoding the input information with the linear transform and the sigmoid function through the condition (43),

$$h=\bar{F}\left(\hat{W}\ast y+\hat{b}\right)$$

(43)

The proposed hybrid capsule network with auto encoder weight parameter is optimized with adaptive equilibrium optimization. Here, the encoder weights (\(\hat{W}\)) and biases (\(\hat{b}\)) are optimized utilizing the hybrid equilibrium optimization procedure. The representation of Hybrid equilibrium optimizer with capsule auto encoder is given in Fig. 2.

Fig. 2

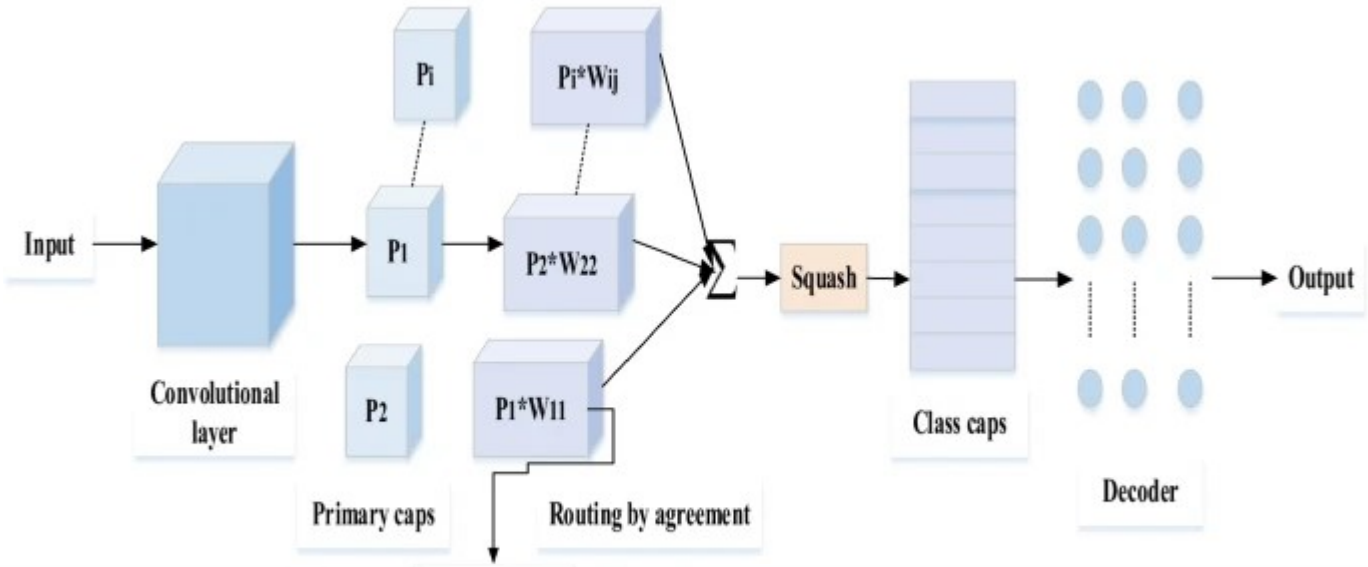

- Convolutional layer: In this stage, convolution operation is performed and the base features are learned from the input datathrough this operation.
- Primary Caps:In this stage, again the same process of the preceding layer is performed and attains more features. Later, the resultant features are given to the squash operator and conserving the alignment and normalizing the length in the range of 0 to 1.The primary caps are routed to the class caps through the dynamic routing approach among the capsules. The contribution of every capsule in the primary capsule layer is computed by the subsequent condition (44),

$${\bar{v}}_{kl}={W}_{lk}\ast {v}_l$$

(44)

Here, v_l represents the output of capsule l, \({\bar{v}}_{kl}\) represents the prediction vector, and W_{lk} represents the weight matrix.

This hybrid equilibrium optimization performs the operation of estimating the equilibrium states of the source and dynamic models. Initially population is introduced for the optimization problem. An initial population of M variables are computed through the condition (45),

$${Z}_k^d={Z}_{\min }+{\bar{R}}_k^d\left({Z}_{\max }-{Z}_{\min }\right),\kern2em k=1,2,.\dots M\kern0.5em and\kern0.74em d=1,2,.\dots D$$

(45)

Moreover, the average locations of the members build to others are described as,

$${M}_{eq, pool}=\left\{{M}_{eq(1)},{M}_{eq(3)},{M}_{eq(3)}.\dots \dots {M}_{eq(average)}\right\}$$

(46)

The correlation among the fitted values of the members in the equilibrium are pool are computed through the condition (47),

$${F}_{M\; eq(1)}\le {F}_{M\; eq(2)}\le {F}_{M\; eq(3)}.\dots \le {F}_{M\; eq(N)}$$

(47)

$${M}_{eq(average)}=\frac{M_{eq(1)}+{M}_{eq(2)}+{M}_{eq(3)}.\dots \dots \dots +{M}_{eq(N)}}{N}$$

(48)

In the exploration phase, every considered fitted values of the particles are related with the values present in the pool of the equilibrium. The optimal weights are then replace the best members in the orders controlled with the condition (47) in the equilibrium pool.

- Exploration and exploitation

In the exploration process, similar solution of dynamic mass balance condition (48) is attained. Here, an exponential term is introduced to control the process.

$$t={\left(1-\frac{I}{I_{\max }}\right)}^{b_2\frac{I}{I_{\max }}}$$

(50)

Here, I represents the iteration and $I_{\max}$ represents the maximum of iteration, and b_2 represents the constant constraining the ability of exploitation. Generation ratio (G) is an important factor utilized in the optimization and it is computed through the condition (51),

$$\overset{\frown }{G}={\overset{\frown }{G}}_0\bar{E}$$

(51)

Here, \({\overset{\frown }{G}}_0\) signifies the initial generation rate factor and it is evaluated with a random vector through the condition (52),

$${\overset{\frown }{G}}_0={R}_V\left({M}_{eq}-\lambda M\right)$$

(52)

Here,

$${R}_V=\left\{\begin{array}{l}0.5{a}_1\kern0.96em {a}_2\ge G\kern0.48em \\ {}0\kern2.04em {a}_2<G\end{array}\right.$$

(53)

In condition (53) a_1 and a_2 represents the arbitrary vectors in the range between of 0 and 1

The attained best locations are considered as best weights in the hybrid capsule auto encoder classifier. The attained weights are updated for the accurate learning of the network.

- Routing through agreement: It does almost similar operation of the max pooling. It selects the information which transfer to the next level. In this step, every capsule performs the operation of predicting the subsequent layer activation according to its length and positioning. The coefficients utilized in the routing process are to compute the connection amongst low and high level capsules through the recurring routing. The agreement among the capsules isdescribed by the multiplication of prediction vector and the pairing coefficient. Then, if the agreement is higher, then the high and low level capsules are connected to each other. Hence, the coefficient pairing will increase else it will decrease. It is computed by the subsequent conditions are,

$${\bar{C}}_{kl}=\frac{e^{d_{kl}}}{\sum \limits_m{e}^{d_{km}}}$$

(55)

$${d}_{kl}={d}_{kl}+u\bar{v}$$

(56)

- Class Caps: After the completion of previous layer operation, digit caps are attained. The squashed vectors characterize the instantiation constraints of every class. The length is depends on the possibility of input fits to particular class.
- Reconstruction stage with decoder: This part comprises of fully connected layers. This stage considers the lengthiest digit caps vectors and utilizes fully connected layers to

(57)

The entity loss is computed through the condition (58)

$${E}_L={M}_L\left(y,{y}^{\ast}\right)$$

(58)

Here, y denotes the input data and y^* represents the output data. Finally, this presented framework provides the accurate identification of normal or mild cognitive impairment or Alzheimer diseased image. The pseudo code of the proposed multi class AD prediction is provided in Algorithm 1.

Algorithm 1: Pseudo code of the proposed multi class AD prediction

Input:

Input image $(\bar{I})$, learning rate $(\overline{\eta})$, and parameters.

Output:

Predicted multi class AD types in input ADNI dataset images

Begin

Pre-process the input image $(\bar{I})$

1. DT based thresholding // Skull stripping
2. normalized linear smoothing and median joint (NLSMJ) filtering// Filtering

Fed the pre-processed images samples to adaptive fuzzy based atom search optimizer

Region segmentation // grey matter (GM), white matter (WM) and cerebrospinal fluid (CSF) region segmentation

GM registration // Improved affine transformation

For image pixels $i=1$ to P_k do

Feature extraction// improved Zernike features and hybrid wavelet walsh features

For layers (K) $:1\rightarrow k-1$ do // here layers K (Convolutional, Primary caps, routing by agreement, class caps, decoder).

Return predicted class labels as AD, normal and MCI in ADNI dataset images.

End

The presented multi class AD prediction process pseudo code is provided in Algorithm 1. The presented approach effectively classifies the input images into AD class, MCI class and CN classes. The performance of the presented approach is examined with various performance metrics and they are discussed in the following results and discussion section.

4 Results and discussion

The presented Alzheimer detection is implemented in MATLAB R2021a platform, Intel i5 processor, and 8GB RAM CPU. Here, ADNI dataset is utilized for the performance examination of the presented work. The performance of the presented technique is examined with the existing support vector machine (SVM), K-nearest neighbour, linear discriminant, decision tree techniques in terms of Accuracy, sensitivity, specificity, PPV, NPV, precision, F1 measure and AUC score. The dataset utilized for the analysis of the presented technique is Alzheimer's disease Neuroimaging initiative (ADNI) dataset. The presented framework classifies the input into Alzheimer's disease (AD) or Cognitive normal (CN) or Mild cognitive impairment (MCI). The ADNI dataset comprises of images with skull and without skull. Both category images are considered in this work for the analysis. The parameters and the hyper parameters used in the values are enhancing the performance of the approach. Here, the presented approach is analysed with a batch size of 50, 100 and 150. Better result is achieved with the batch size 50. Furthermore, the dropout value of presented approach is 0.2. The presented technique when using the dropout 0.2 is get better performance. Similarly, the experimental setup is tested

images of peoples age from 55 to 90. The database comprises of cognitive normal (CN) old age

peoples, and the peoples with early otherwise late Mild cognitive impairment (MCI) and the peoples with early Alzheimer's disease (AD) categories. The ADNI was funded by the national institute on aging and the bio medical imaging and Engineering. ADNI is a standard dataset used for predicting the different classes like AD, MCI and normal data effectively. The subjects were selected from around 50 sites across the U.S and Canada. Moreover, the size of images in this dataset are 227×227.

Training and testing sets: The considered ADNI dataset comprises of1167 images totally. They are separated into training and testing data in the ratio of 70% and 30%. Here, the 817 images are considered for the training process and the 350 images are considered for the testing process.

The input images of ADNI dataset is used for the prediction of multi AD classes using the hybrid deep learning approach. Initially, input sample images with skull are considered for the process. The input sample images of ADNI dataset is depicted in Fig. 3, outcome of skull stripped images are depicted in Fig. 4, outcome of filtered images are depicted in Fig. 5, segmented CSF, WM, GM regions are depicted in Fig. 6, and registered images are depicted in Fig. 7.

Fig. 3

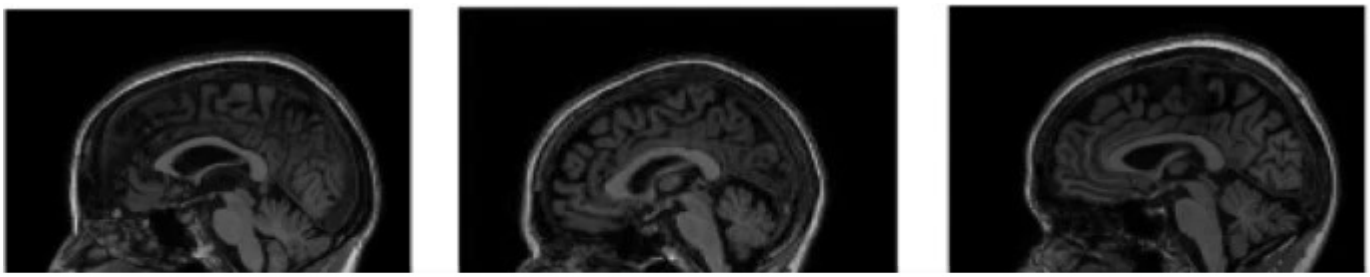

Fig. 4

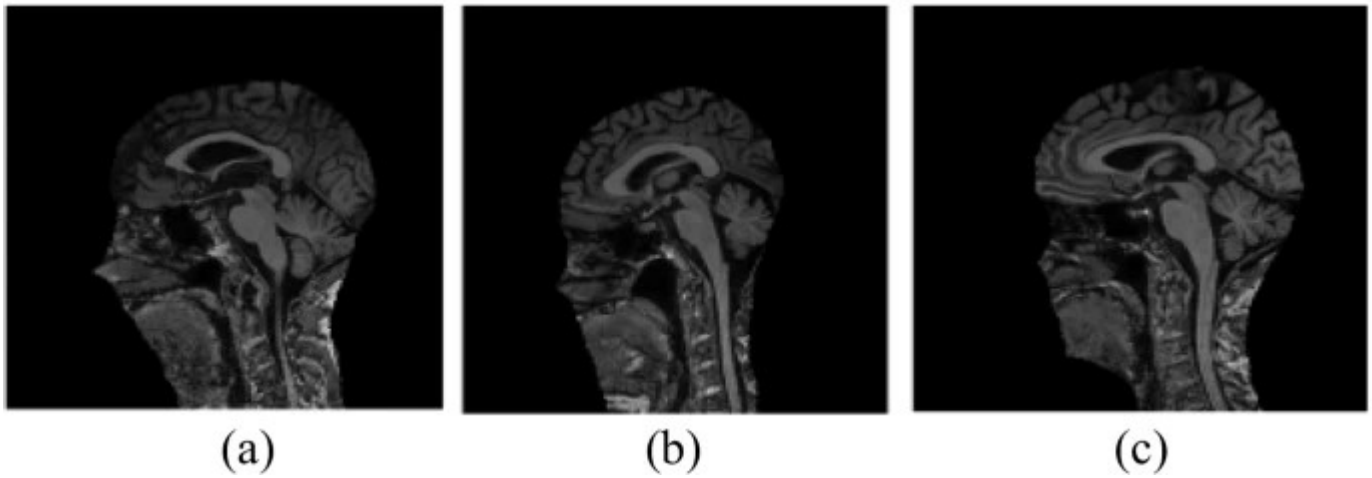

Outcome of skull stripped images (a) AD (b) normal (c) MCI

Fig. 5

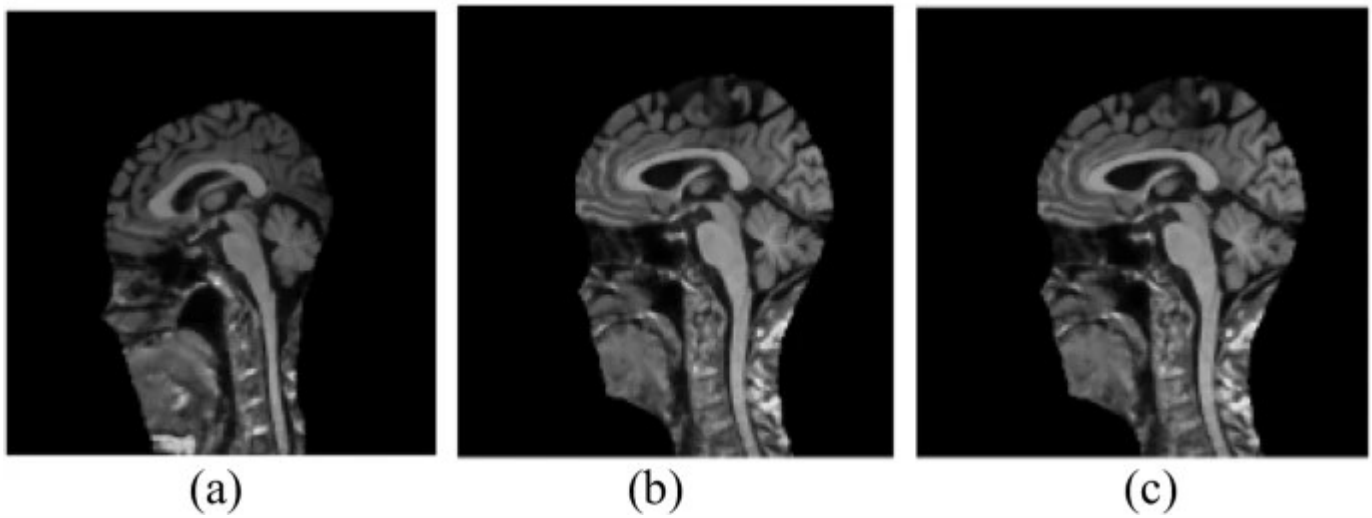

(a)

(b)

(c)

Outcome of segmented CSF, White matter, Grey matter regions of (a) AD (b) Normal (c) MCI

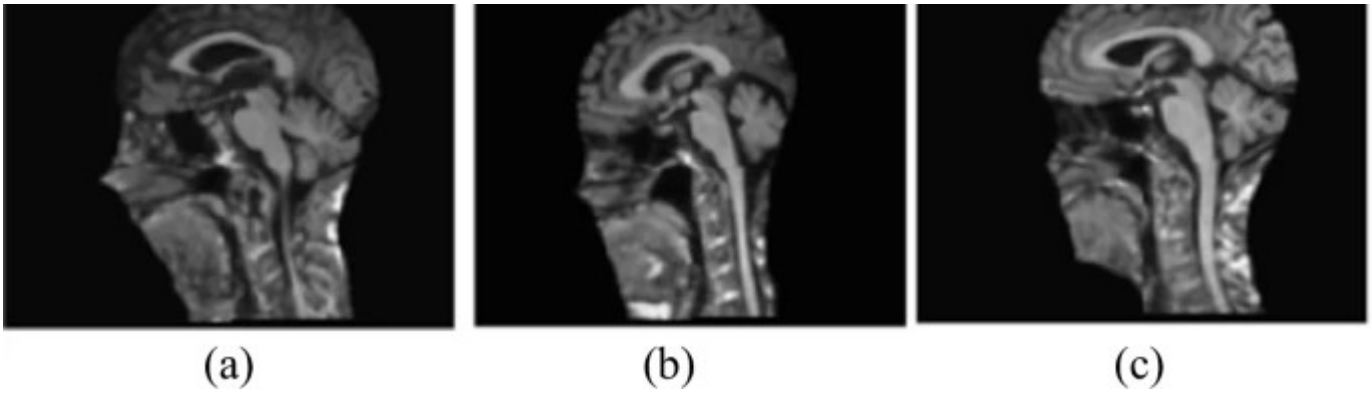

Outcome of registered images of (a) AD (b) normal (c) MCI

Another set of sample images taken from ADNI dataset without skull region is depicted in the following images. The input sample images of ADNI dataset without skull region are depicted in Fig. 8. The outcome of filtered images are depicted in Fig. 9, segmented CSF, WM, GM regions are depicted in Fig. 10, and registered images are depicted in Fig. 11.

Fig. 8

Fig. 9

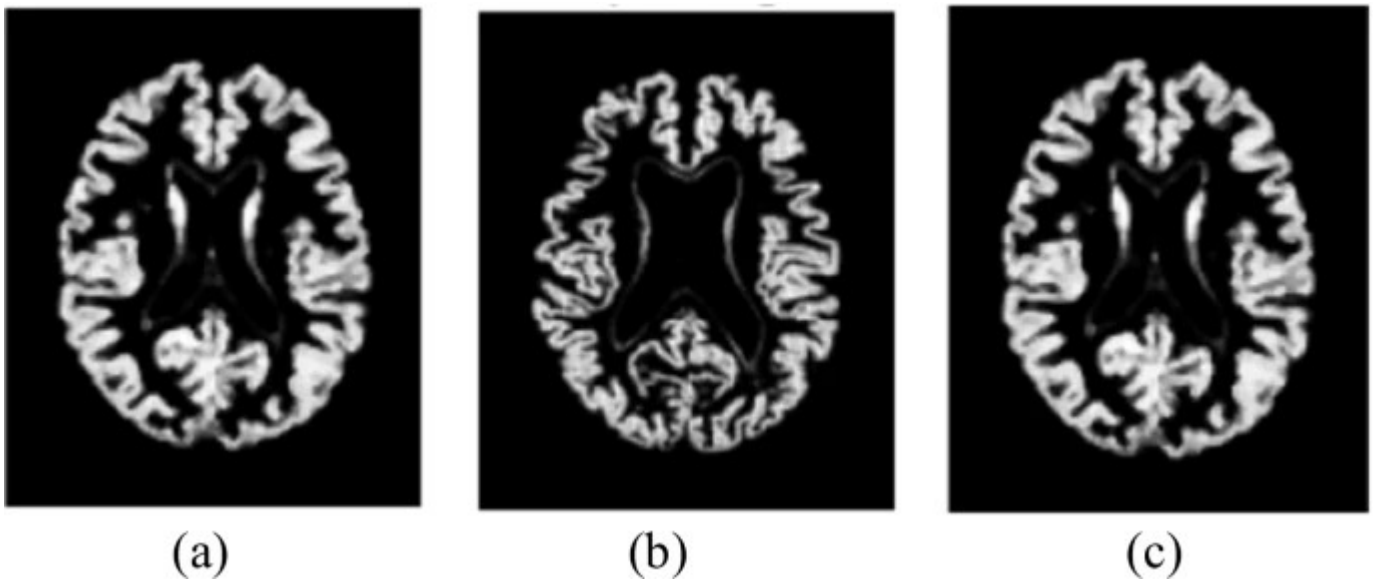

Outcome of filtered input images (a) AD (b) normal (c) MCI

Fig. 10

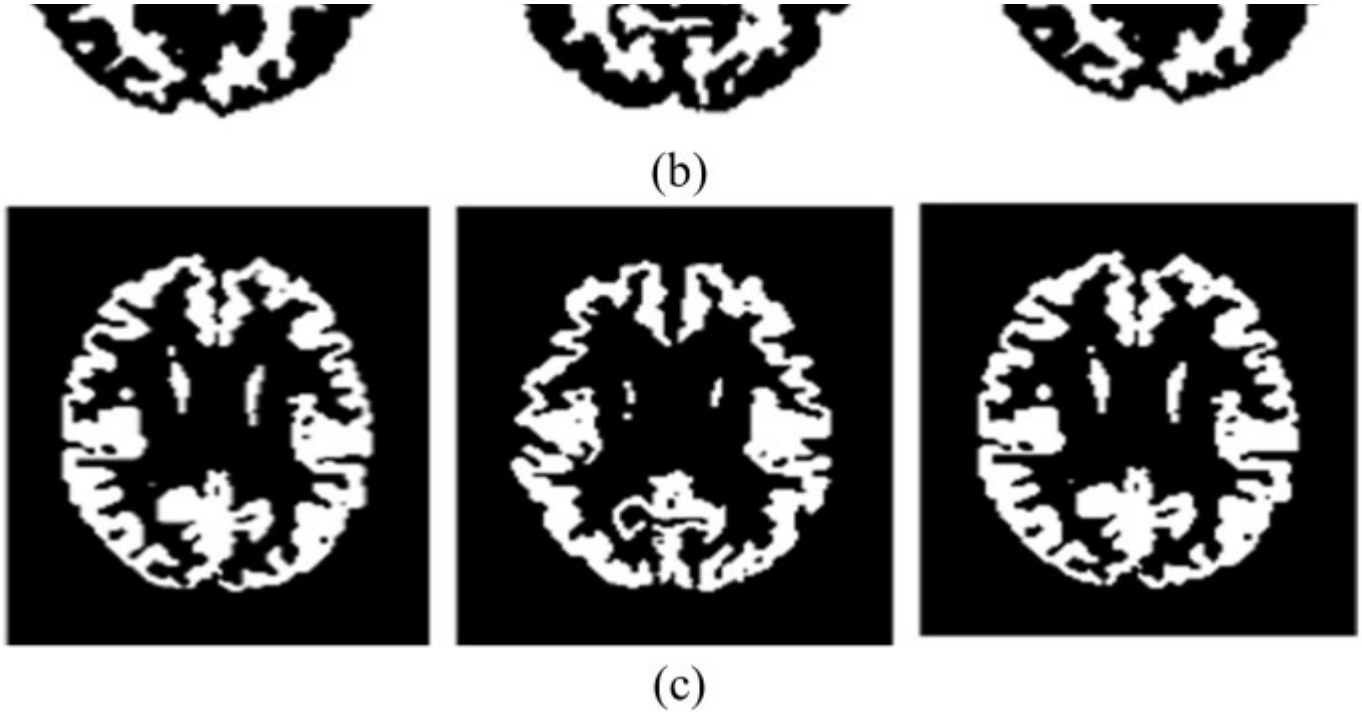

Outcome of segmented CSF, White matter, Grey matter regions of (a) AD (b) Normal (c) MCI

Fig. 11

In this section, effective performance measures like Accuracy, Sensitivity, specificity, ROC

(Receiver operating characteristic) curve, AUC (Area under the curve) score, F-measure, and Precision are evaluated to examine the performance of presented technique.

- Accuracy (A_y)

This represents the accurately predicted classes and it is expressed through the condition (59),

$${A}_y=\frac{T_{positive}+{T}_{negative}}{T_{positive}+{T}_{negative}+{F}_{positive}+{F}_{negative}}$$

(59)

Here, A_y signifies the accuracy, $T_{positive}$ signifies the true positive, $T_{negative}$ signifies the true negative, $F_{positive}$ signifies the false positive and $F_{negative}$ signifies the false negative.

- Sensitivity (S_y)

This represents the total number of original positives which are correctly categorized. It is computed through the condition (60),

$${S}_y=\frac{T_{positive}}{T_{positive}+{F}_{negative}}$$

(60)

- Specificity (S_p)

- Precision (P_r)

This measures the positives which are correctly identified among all the positives and it is computed through the condition (62),

$${P}_r=\frac{T_{positive}}{T_{positive}+{F}_{positive}}$$

(62)

- F-measure (F_{score})

F-measure is estimated by the harmonic mean of the precision and sensitivity. This evaluation is expressed through the condition (63),

$${F}_{score}=2\ast \frac{S_y\ast {P}_r}{S_y+P}$$

(63)

- Receiver operating characteristic (ROC) measure

This performance evaluation evaluates the effectiveness of the presented technique. It is accomplished with true positive rate (t_{PR}) against the false positive rate (f_{PR}). The TPR and FPR are characterized through the condition (64) and condition (65),

$${t}_{PR}=\frac{T_{positive}}{T_{positive}+{T}_{negative}}$$

(64)

- AUC score

This performance measure is the evaluation ranking probabilityof chosen positive instance higher than a negative instance. It is computed through the condition (66),

$${AUC}_{score}={~}^{\left({S}_y+{S}_p\right)}\!\left/ \!\!{~}_{2}\right.$$

(66)

Here, S_y represents the sensitivity, S_y represents the specificity.

4.2 Performance analysis

In this section, performance of the presented approach is examined with the existing techniques. Here, ADNI dataset utilized for the examination of the presented work with various performance measures. The confusion matrix attained for presented work with three classes is depicted in Fig. 12.

Fig. 12

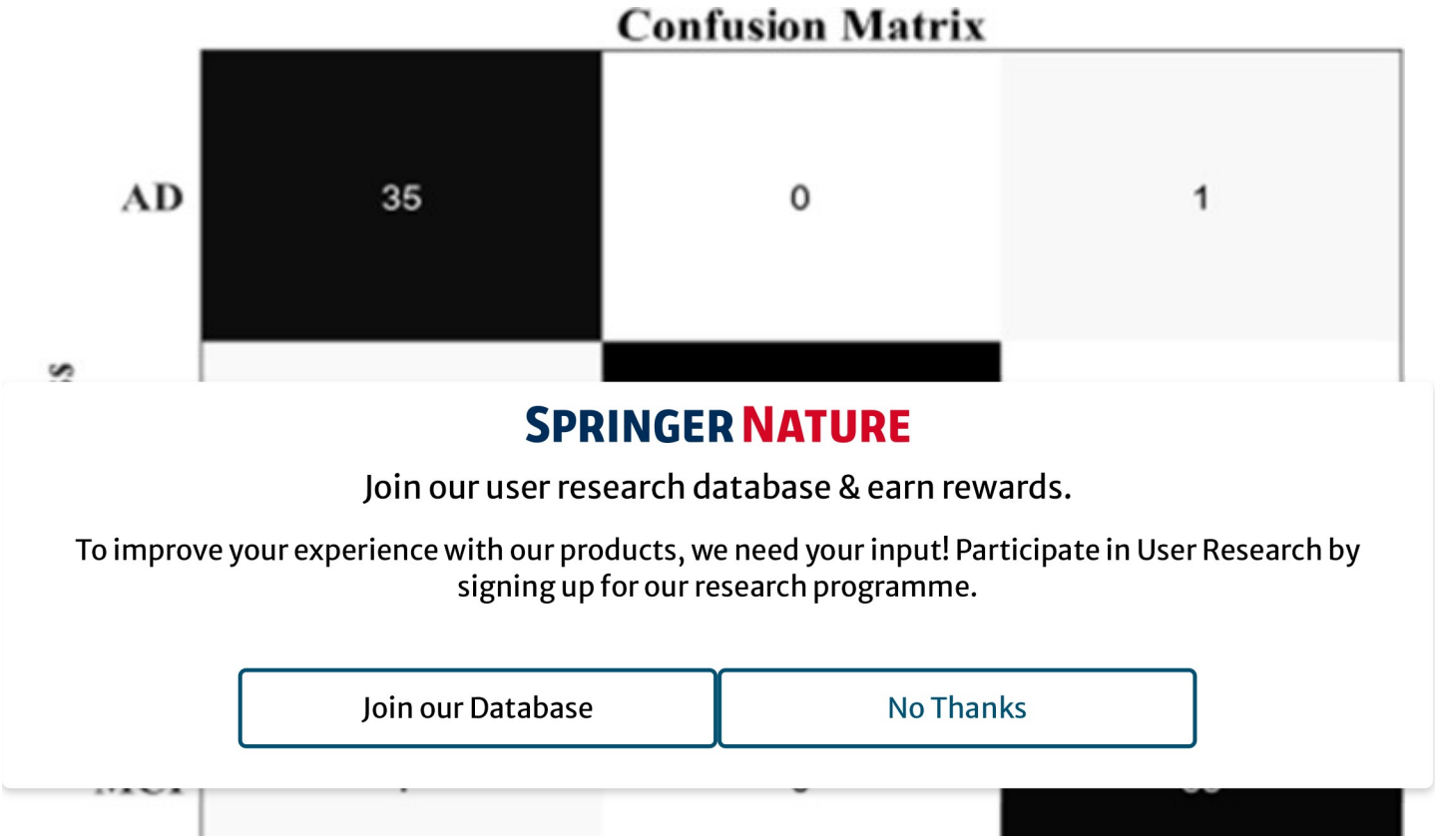

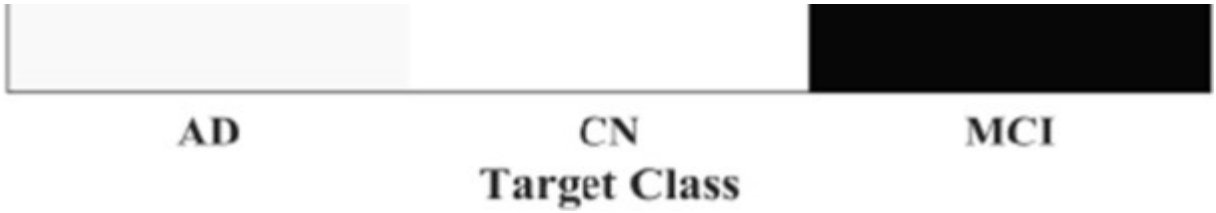

Confusion matrix output with AD, CN and MCI classes

The comparison analysis of the presented methodology in regards of accuracy is specified in Table 1.

Table 1 Comparison analysis of different performances with ADNI dataset

In Table 1, the performance analysis of the presented technique is compared with the existing Curvelet transform based K-nearest neighbourhood (CuT+KNN), Adaboost, Random forest (RF), Dual tree complex wavelet transform with KNN (DTCWT-KNN) [1],KNN (K-nearest neighbourhood), Support vector machine (SVM), Linear discriminant, Decision tree [27]approaches. Here, the presented approach attains improved accuracy than the other existing approaches. The performance in regards of accuracy is represented in Fig. 13.

Fig. 13

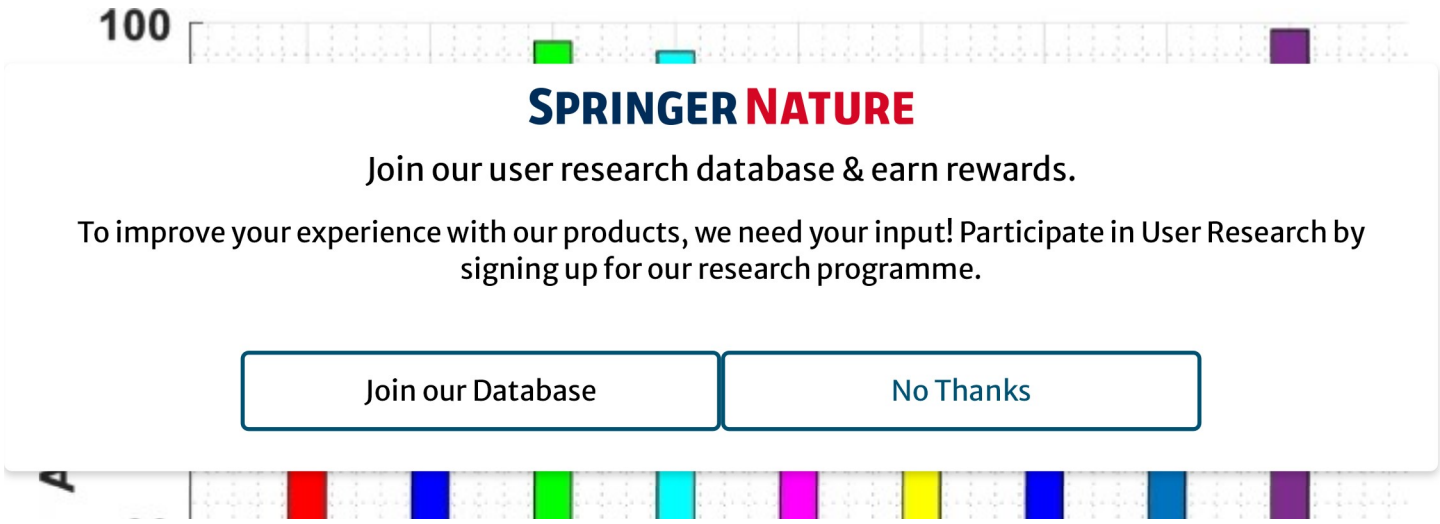

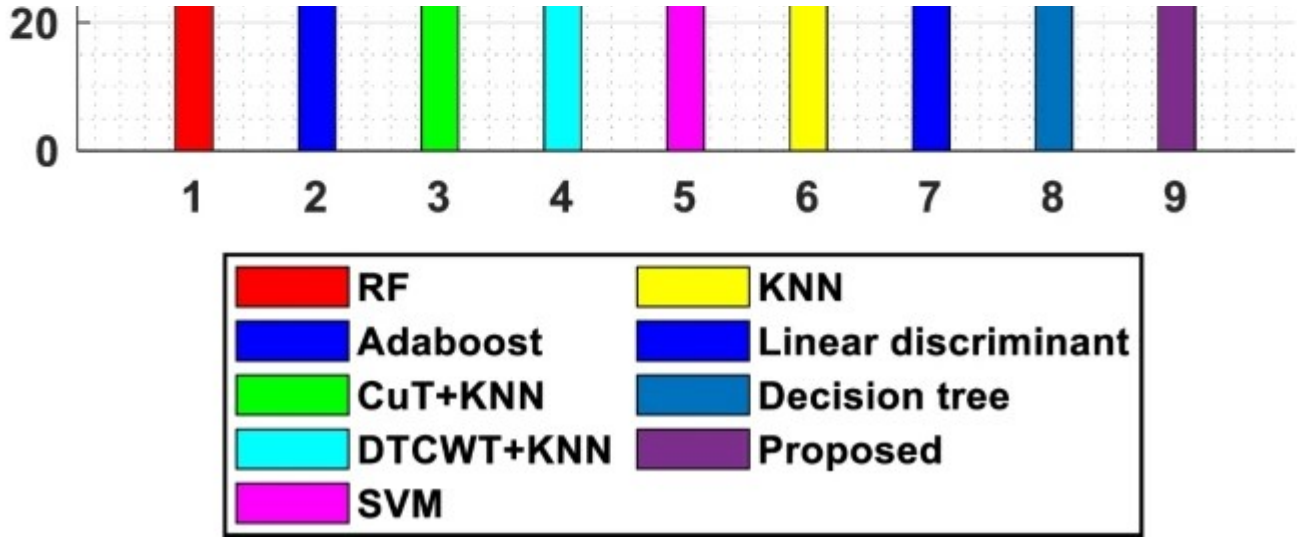

Performance analysis in regards of accuracy

In Fig. 13, comparison analysis on accuracy performance is depicted. The proposed approach attains enhanced accuracy (98.21%) than the other previously available techniques like CuT+KNN (96.97%), Adaboost (83.3%), RF (83.33%), DTCWT-KNN (95.45%) [1], KNN (76.52%), Decision tree (69.6%), SVM (76.32%), and Linear discriminant (71.4%) [17]. Accuracy performance for each separate AD, MCI and CN class is depicted in Fig. 14.

Fig. 14

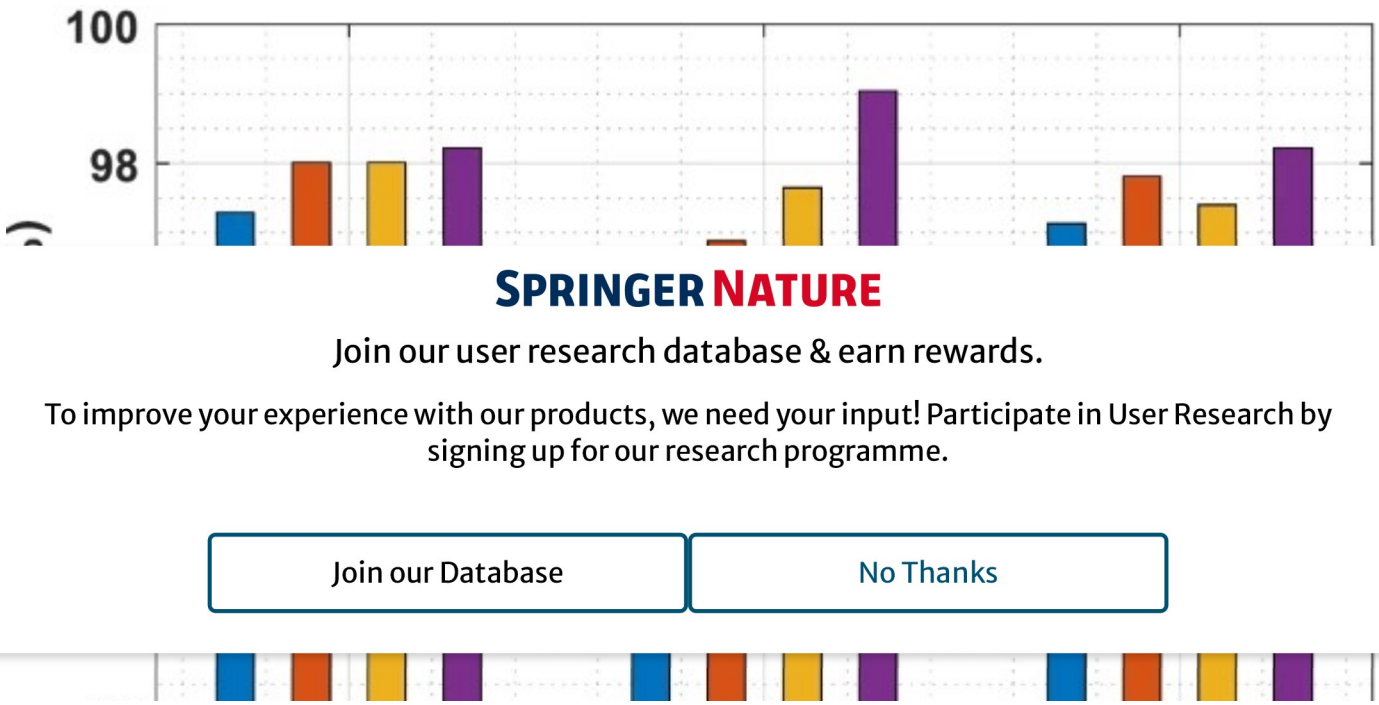

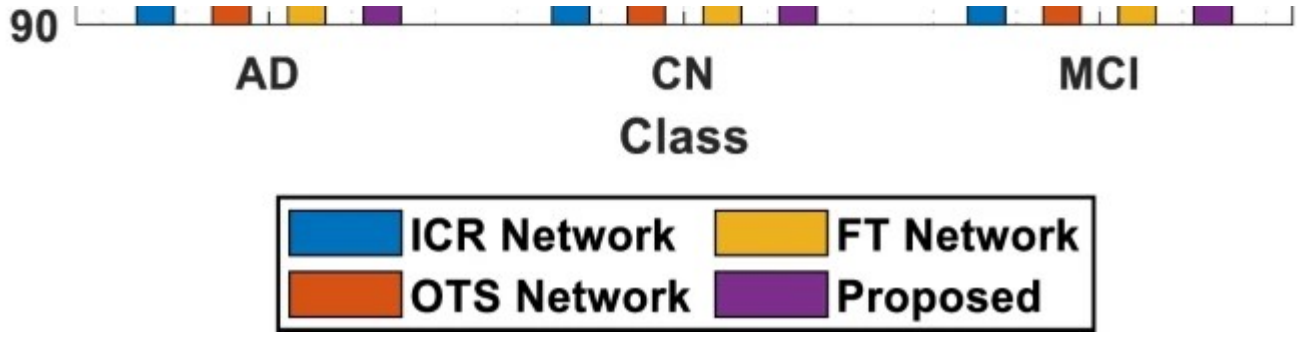

Performance analysis in regards of accuracy of each class AD, CN, MCI

In Fig. 14, accuracy performance of AD, CN and MCI classes are depicted. The presented approach accuracy performance is examined with the different existing approaches like off the shelf (OTS) network, 1CR (1 channel Resnet-18) network and Fine tuning (FT) network [27]. This proved that the accuracy performance on each separate class is significantly higher than the existing approaches. In each class, the presented methodology attains better performance than the other current techniques. The sensitivity performance of the presented approach is depicts in Fig. 15.

Fig. 15

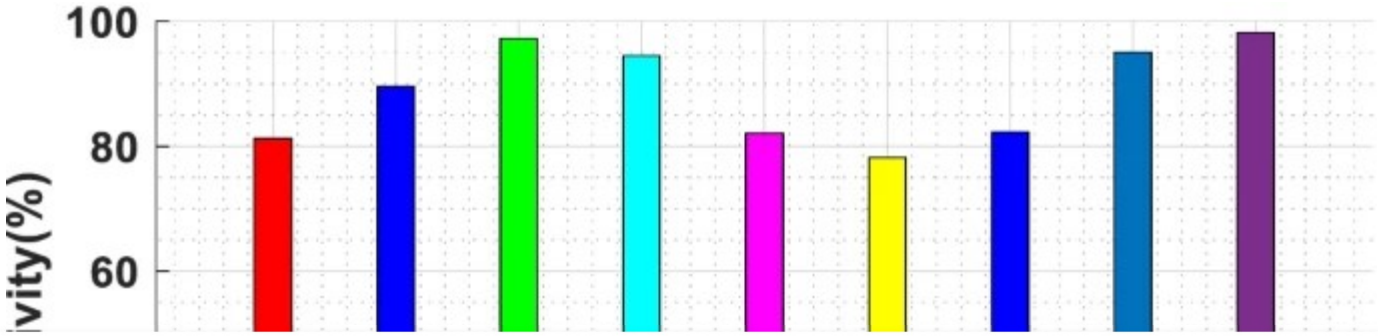

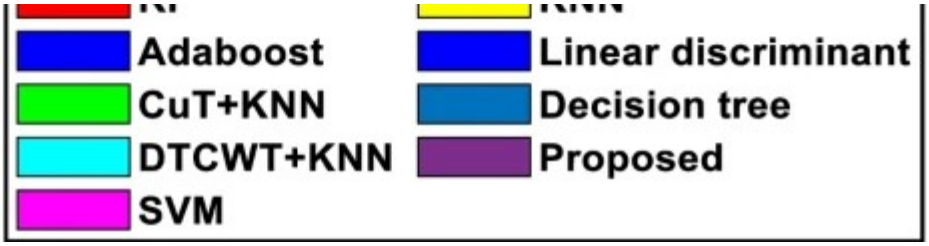

Comparison analysis in regards of sensitivity

In Fig. 15, comparison analysis on sensitivity performance is provided. The attained sensitivity result of the developed technique is 97.31%. This clearly depicts that the performance of presented approach attains improved performance than the existing RF (81.25%), CuT+KNN (97.22%), Adaboost (89.58%), DTCWT+KNN (94.44%) [1], KNN (78.2%), linear discriminant (82.3%), SVM (82.1%), and decision tree (95%) [17]. Moreover, the comparison analysis in regards of specificity is illustrated in Fig. 16.

Fig. 16

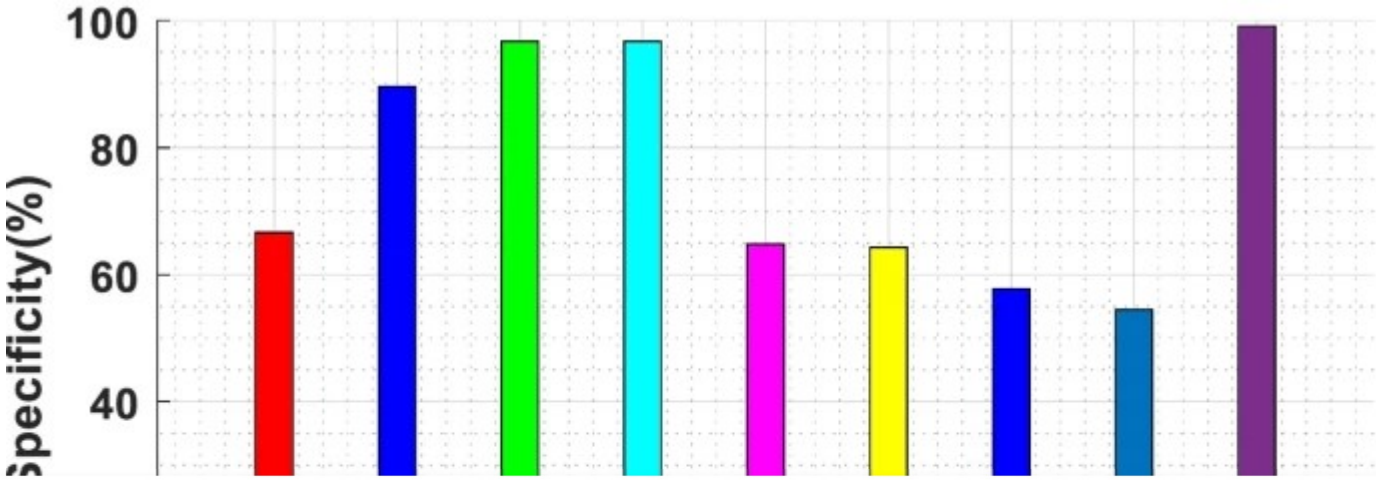

Comparison analysis in regards of specificity

The Fig. 16 provides the comparison analysis on sensitivity. This illustrates that the sensitivity performance of the presented approach (98.64%) attains significant improvement than the CuT+KNN (96.67%), Adaboost (89.58%),RF(66.66%), DTCWT+KNN (96.67%) [1],linear discriminant (57.8%), KNN (64.3%), SVM (64.8%), and decision tree (54.5%) [17]. Furthermore, the precision performance is depicted in Fig. 17.

Fig. 17

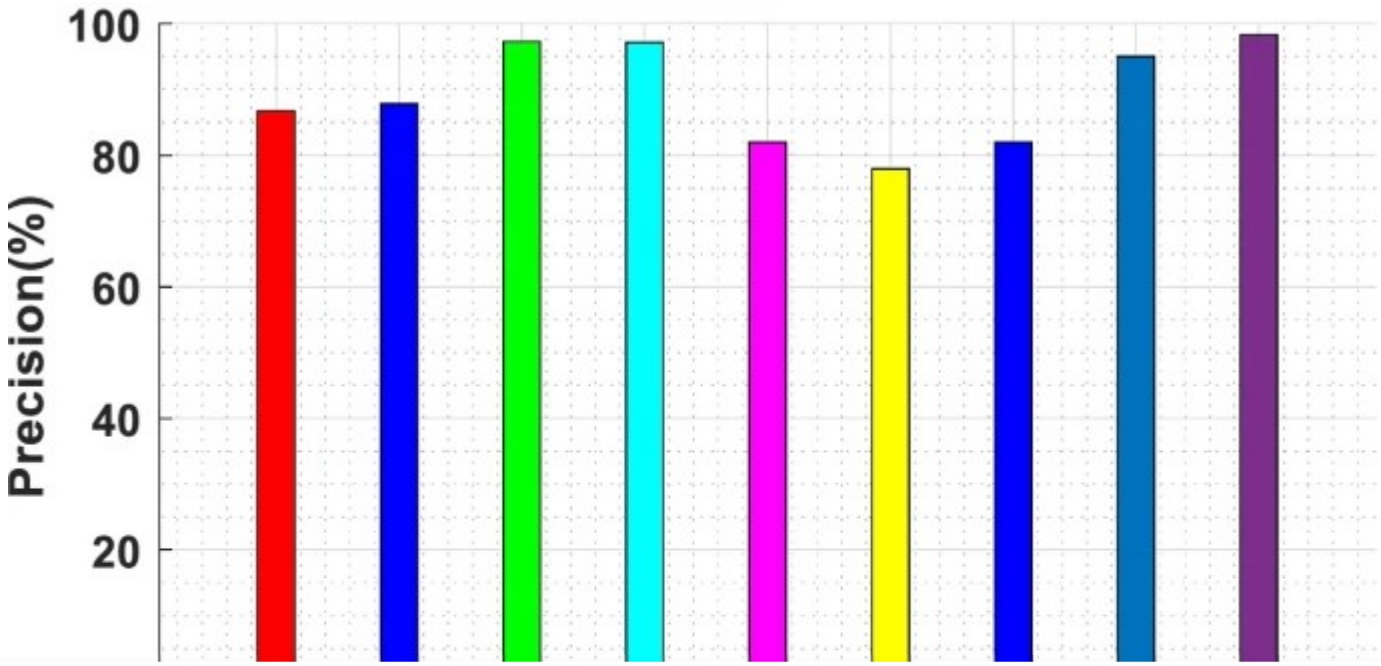

Comparison analysis in regards of precision

In Fig. 17, performance examination on precision is depicted. The precision performance illustrated in Fig. 17 proves that the presented methodology (97.45%) attains increased performance than the existing approachesare RF (86.66%), Adaboost (87.75%), CuT+KNN, DTCWT+KNN (97.14%) [1], linear discriminant (56%), SVM (82%), KNN (78%), and decision tree (94%) [17]. The negative predictive value (NPV) performance of the introduced technique is illustrated in Fig. 18.

Fig. 18

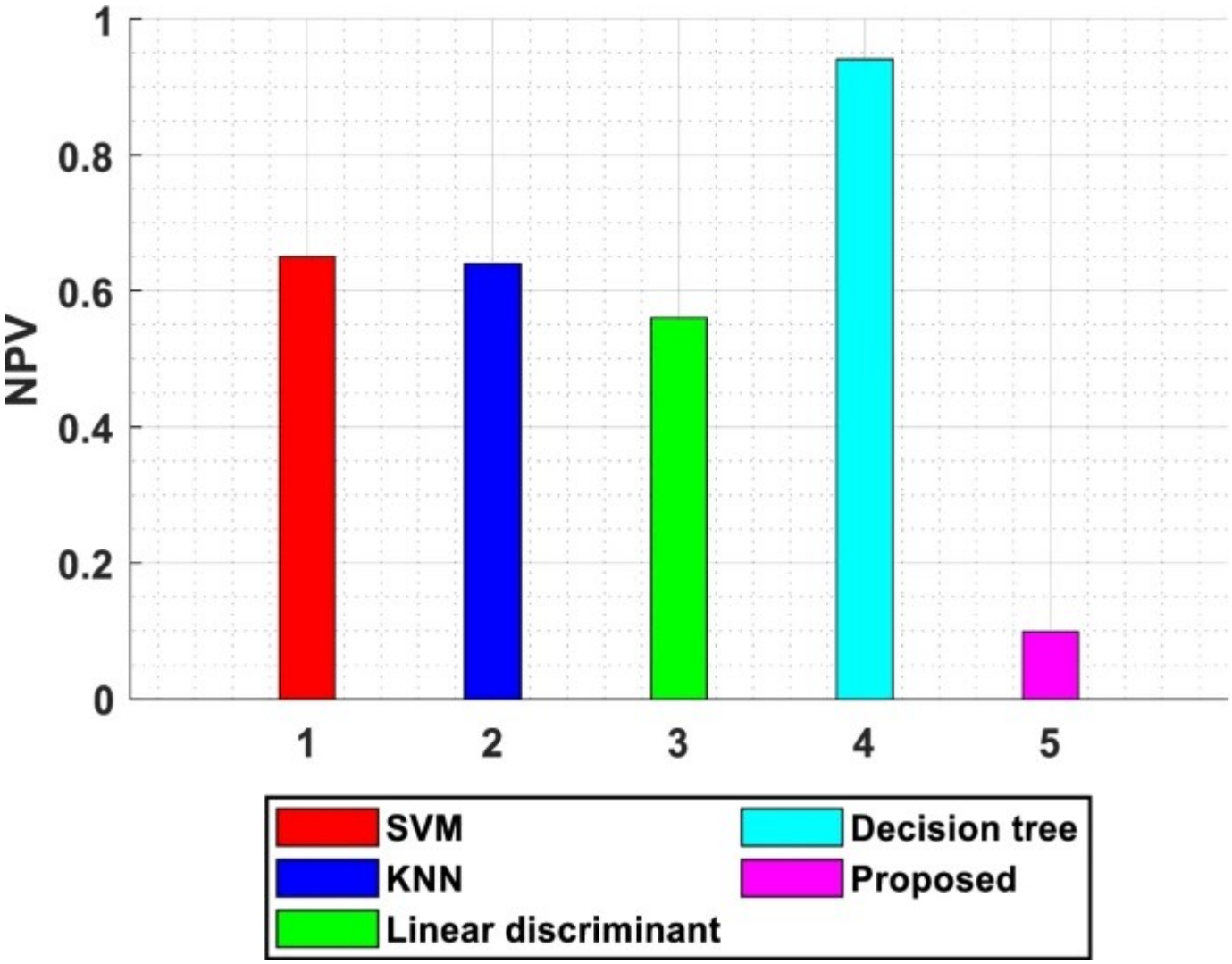

Comparison analysis in regards of NPV

In Fig. 18, comparison analysis on NPV is illustrated. The NPV performance depicted in Fig. 18

Table 2 Comparisonanalysis of AUC with ADNI dataset

In Table 2, the performance analysis on AUC is mentioned. The presented approach AUC outcome is 98.29%, which is the significant improvement than the different existing methodologieslike deep learning (74.66%), Multi-kernel SVM (76.8%), Bayesian (79.5%), Random forest (90.2%), Independent component analysis (ICA) (80.8%), domain transfer SVM (DTSVM) (84.8%), learning network (93.2%), Feature ranking (75.08%), and Multi-class SVM-GS (Grid search) (93.59%) [13]. The AUC performance of the presented work is examined with the previous approaches aredepicted in Fig. 19.

Fig. 19

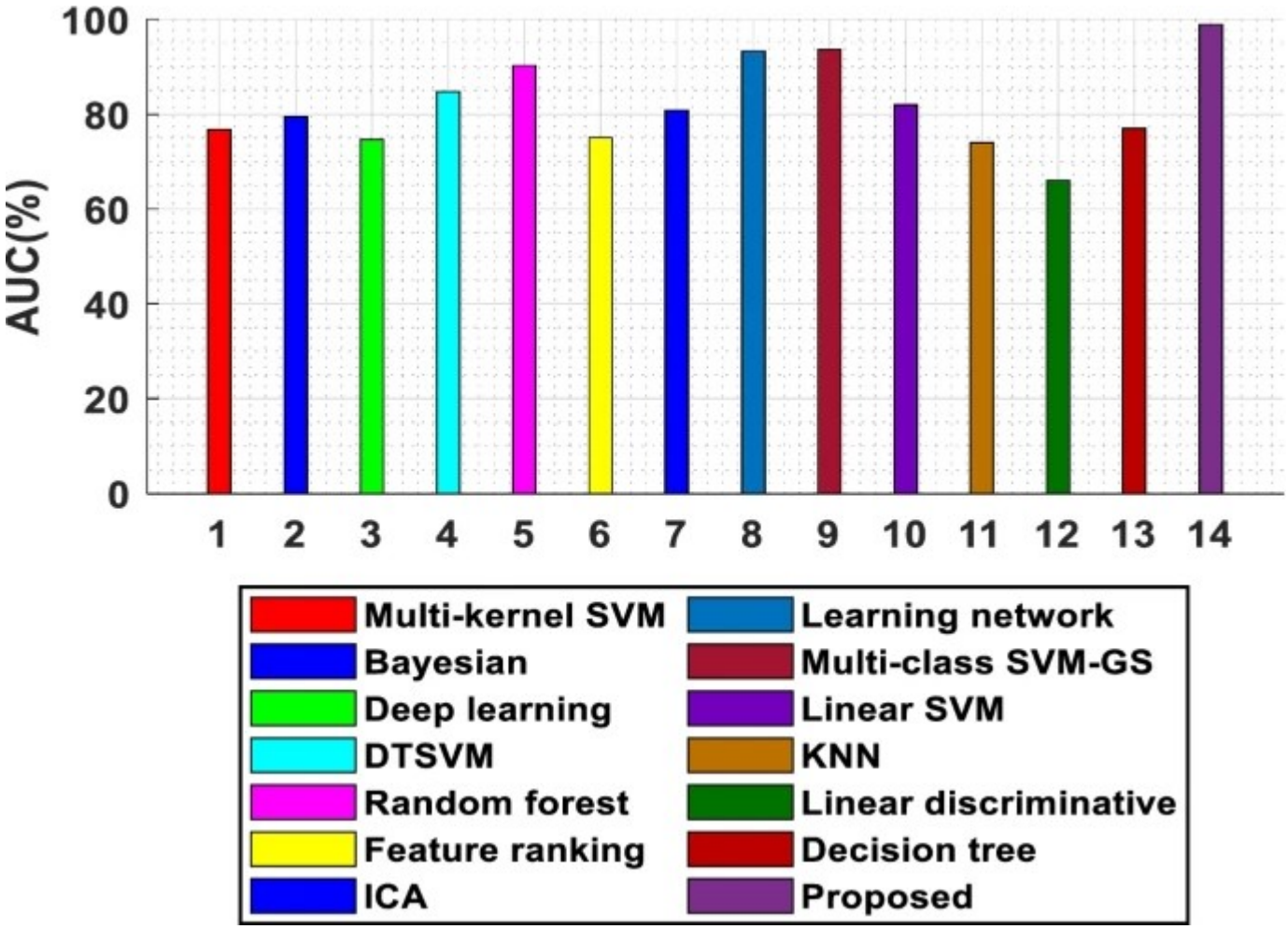

Comparison analysis in regards of AUC (%)

The Fig. 19, demonstrates the AUC performance comparison. This illustrates that the presented methodology attains enhanced AUC (98.29%) performance than deep learning (74.66%), domain transfer SVM (DTSVM) (84.8%), learning network (93.2%), Multi-kernel

Fig. 20

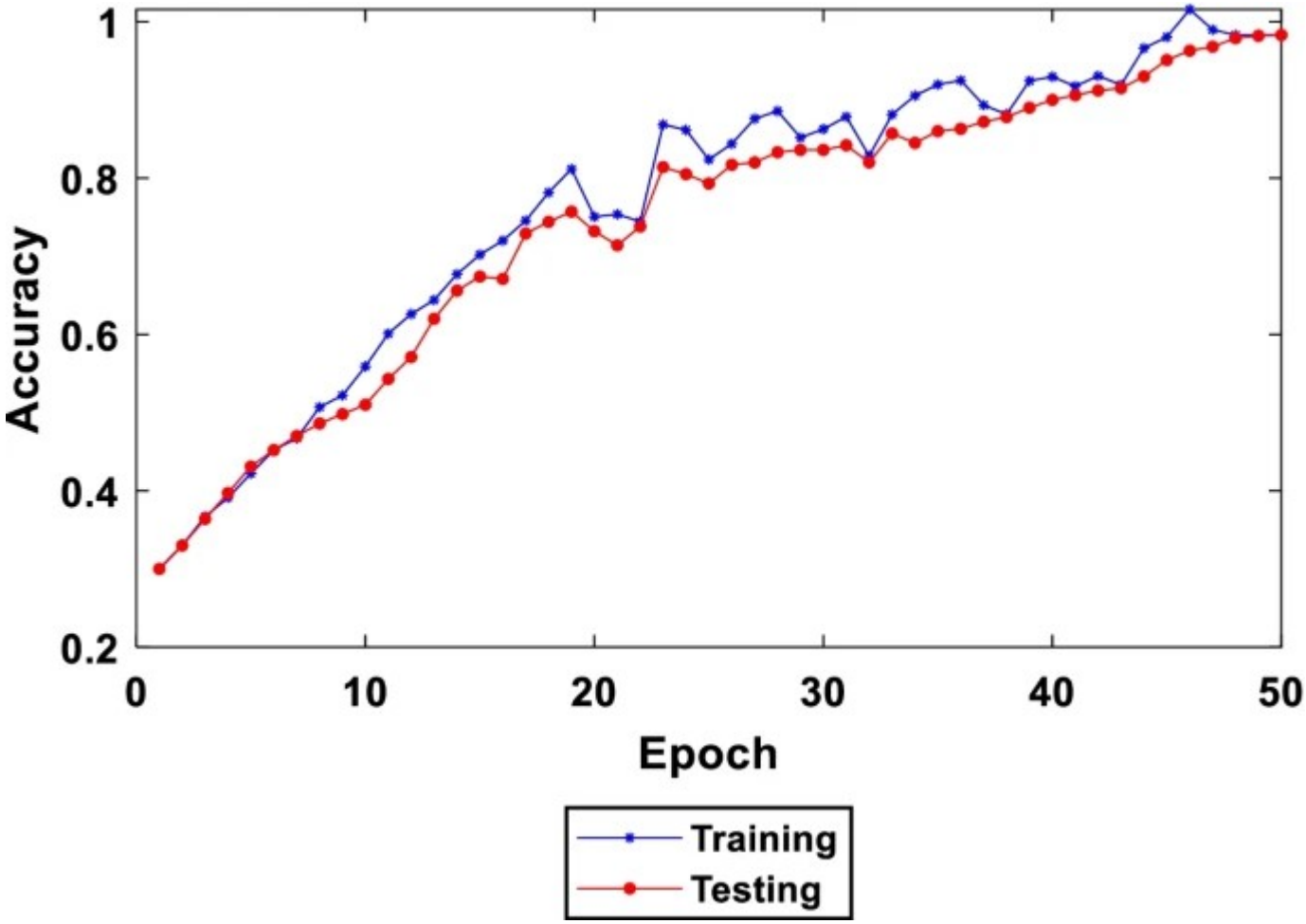

Training and testing accuracy with the number of epochs

In Fig. 20, the accuracy performance of training and testing process with the number of epochs are demonstrated. The technique performance is analysed with epoch size 50. The better performance on accuracy is achieved by selecting the epoch size 50. Moreover, the

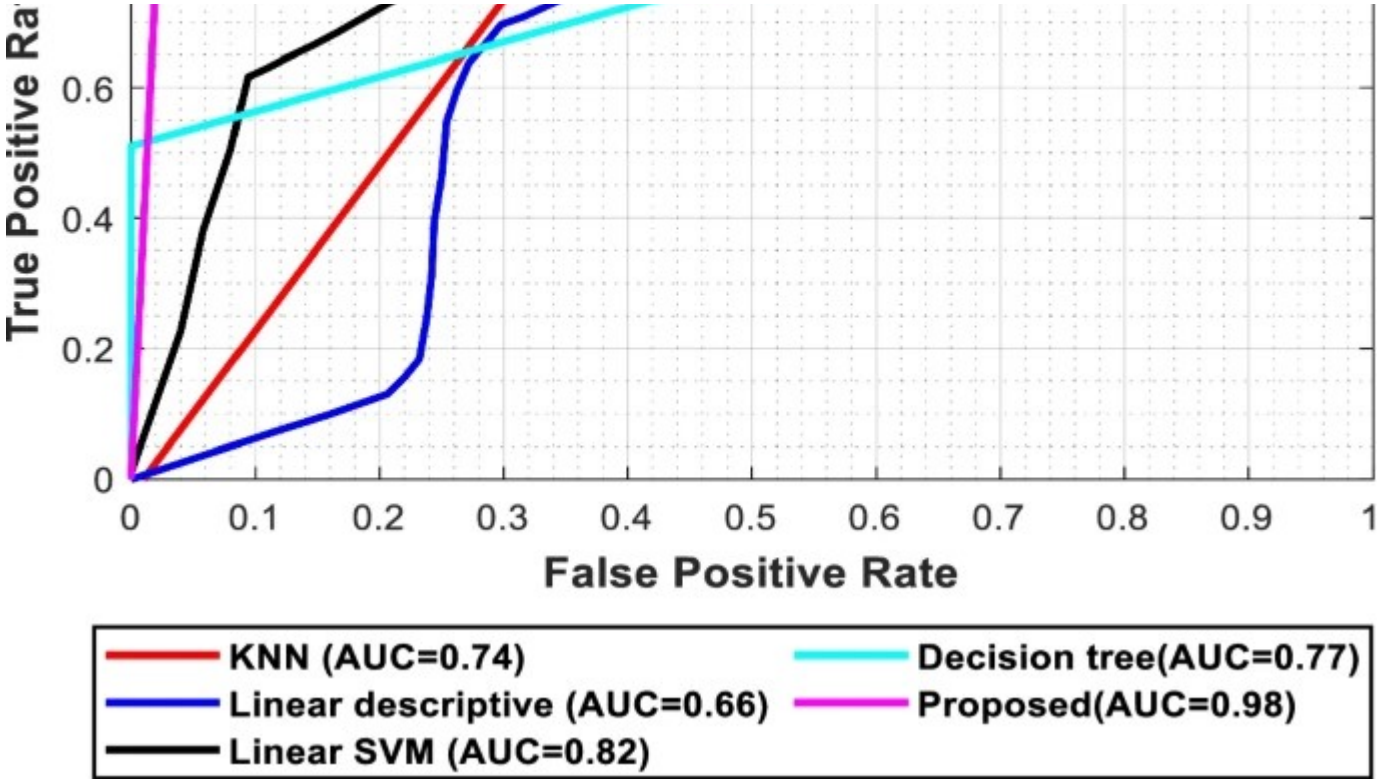

Comparison analysis in regards of ROC

In Fig. 21, comparison analysis on ROC is displayed. From the Fig. 21,it is clearly depicts that the presented approach results better performance in ROC than the existing Linear SVM (0.82), KNN (0.74), linear discriminative (0.66), Decision tree (0.77) [17] approaches. The ROC curve of the presented approach proved that the proposed HEOCAE deep learning approach achieved an enhanced performance than the existing approaches. Furthermore, the comparison analysis in regards of F-measure is illustrated in Fig. 22.

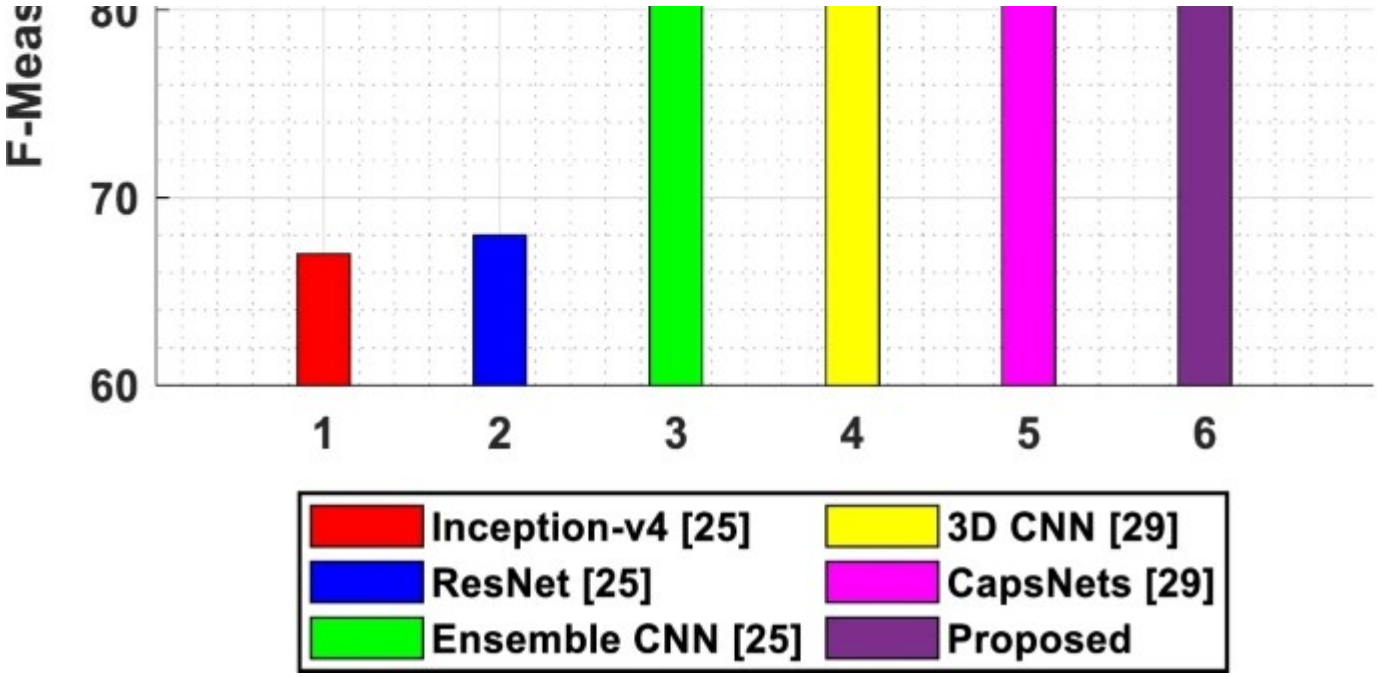

Comparison analysis in regards of F-measure

In Fig. 22, comparison demonstration on F-measure is depicted. The F-measure performance of the presented methodology is analysed with the existing Inception-v4 (71%), Ensemble CNN (92%) and ResNet (75%) [15]. Moreover, the presented approach attains 97.37% of F-measure which is the great improvement than the existing techniques in performance validation.

The presented approach provides enhanced performance in AD prediction. The presented methodology performance is compared with the different existing approaches in terms of different performance metrics like accuracy, sensitivity, specificity, F1 measure, NPV, precision, and AUC score. The examined results proved that the presented methodology

5 Conclusion

This paper presented an improved Alzheimer detection framework with hybrid equilibrium optimizer with capsule auto encoder framework. The input image is pre-processed with NLSMJ filtering technique for enhancing the image and the GM, WM, CSF regions are extracted using adaptive fuzzy based atom search optimization. Moreover, the segmented GM is registered with the pre-processed image. Combined effective features are extracted and selected using adaptive rain optimization. Finally, hybrid equilibrium optimizer with capsule auto encoder is detecting the AD, MCI and CN classes. The presented work performance is examined with the ADNI dataset. Moreover, the performance of the presented technique is examined with the existing support vector machine (SVM), K-nearest neighbour, linear discriminant, decision tree techniques in terms of different performance measures. The presented technique attaining enhanced performances in Accuracy (98.21%), sensitivity (97.31%), specificity (98.64%), NPV (0.098), precision (97.45%), F1 measure (97.37%) and AUC score (98.29%) than the existing techniques. In future work, more classification stages of Alzheimer's disease can be found by using effective deep learning techniques. Moreover, other different performance metrics can be examined to verify the effectiveness of the Alzheimer's prediction.

References

1. Acharya UR, Fernandes SL, WeiKoh JE, Ciaccio EJ, Fabell MKM, Tanik UJ, Rajinikanth V, Yeong CH (2019) Automated detection of Alzheimer's disease using brain MRI images–a study with various feature extraction techniques. J Med Syst 43(9):1–14

3. Altaf T, Anwar SM, Gul N, Majeed MN, Majid M (2018) Multi-class Alzheimer's disease classification using image and clinical features. Biomed Signal Process Control 43:64–74

Article Google Scholar

4. Amini M, Moradi A, Jamshidi M, Ouchani M (2021) Single and combined neuroimaging techniques for Alzheimer's disease detection. Comput Intell Neurosci 2021:1–22

Article Google Scholar

5. Baskar D, Jayanthi VS, Jayanthi AN (2019) An efficient classification approach for detection of Alzheimer's disease from biomedical imaging modalities. Multimed Tools Appl 78(10):12883–12915

Article Google Scholar

6. Billones CD, Demetria OJLD, Hostallero DED, Naval PC (2016) DemNet: a convolutional neural network for the detection of Alzheimer's disease and mild cognitive impairment. In: 2016 IEEE region 10 conference (TENCON). IEEE, pp 3724–3727

Chapter Google Scholar

7. Chen K, Franko K, Sang R (2021) Structured model pruning of convolutional networks on tensor processing units. arXiv preprint arXiv:2107.04191

Implications for prevention of Alzheimer's disease. Curr Epidemiol Rep 7(2):68–76

Article Google Scholar

10. Duraisamy B, Shanmugam JV, Annamalai J (2019) Alzheimer disease detection from structural MR images using FCM based weighted probabilistic neural network. Brain Imaging Behav 13(1):87–110

Article Google Scholar

11. Feng J, Zhang S-W, Chen L, Xia J (2021) Alzheimer's disease classification using features extracted from nonsubsampled contourlet subband-based individual networks. Neurocomputing 421:260–272

Article Google Scholar

12. Grassi M, Rouleaux N, Caldirola D, Loewenstein D, Schruers K, Perna G, Dumontier M (2019) A novel ensemble-based machine learning algorithm to predict the conversion from mild cognitive impairment to Alzheimer's disease using socio-demographic characteristics, clinical information, and neuropsychological measures. Front Neurol 10:756

Article Google Scholar

13. Gupta Y, Lama RK, Kwon G-R, Weiner MW, Aisen P, Weiner M, Petersen R et al (2019) Prediction and classification of Alzheimer's disease based on combined features from apolipoprotein-E genotype, cerebrospinal fluid, MR, and FDG-PET imaging biomarkers

informatics. Springer, Cham, pp 213–222

Chapter Google Scholar

15. Islam J, Zhang Y (2018) Brain MRI analysis for Alzheimer's disease diagnosis using an ensemble system of deep convolutional neural networks. Brain Inform 5(2):1–14

Article Google Scholar

16. Islam J, Zhang Y (2018) Brain MRI analysis for Alzheimer's disease diagnosis using an ensemble system of deep convolutional neural networks. Brain Inform 5(2):2

Article Google Scholar

17. Janghel RR, Rathore YK (2020) Deep convolution neural network based system for early diagnosis of Alzheimer's disease. IRBM 42:258–267

Article Google Scholar

18. Khan RU, Tanveer M, Pachori RB (2021) A novel method for the classification of Alzheimer's disease from normal controls using magnetic resonance imaging. Expert Syst 38(1):e12566

Article Google Scholar

19. Kruthika KR, Maheshappa HD (2019) CBIR system using capsule networks and 3D CNN

20. Lee G, Nho K, Kang B, Sohn K-A, Kim D (2019) Predicting Alzheimer's disease progression using multi-modal deep learning approach. Sci Rep 9(1):1–12

Google Scholar

21. Liu C-F, Padhy S, Ramachandran S, Wang VX, Efimov A, Bernal A, Shi L et al (2019) Using deep Siamese neural networks for detection of brain asymmetries associated with Alzheimer's disease and mild cognitive impairment. Magn Reson Imaging 64:190–199

Article Google Scholar

22. Liu M, Li F, Yan H, Wang K, Ma Y, Shen L, Xu M (2020) A multi-model deep convolutional neural network for automatic hippocampus segmentation and classification in Alzheimer's disease. NeuroImage 208:116459

Article Google Scholar

23. Mehmood A, Maqsood M, Bashir M, Shuyuan Y (2020) A deep siamese convolution neural network for multi-class classification of Alzheimer disease. Brain Sci 10(2):84

Article Google Scholar

24. Nawaz A, Anwar SM, Liaqat R, Iqbal J, Bagci U, Majid M (2021) Deep convolutional neural network based classification of Alzheimer's disease using MRI data. arXiv preprint arXiv:2101.02876

26. Poloni KM, de Oliveira IAD, Tam R, Ferrari RJ (2021) Brain MR image classification for Alzheimer's disease diagnosis using structural hippocampal asymmetrical attributes from directional 3-D log-Gabor filter responses. Neurocomputing 419:126–135

Article Google Scholar

27. Ramzan F, Khan MUG, Rehmat A, Iqbal S, Saba T, Rehman A, Mehmood Z (2020) A deep learning approach for automated diagnosis and multi-class classification of Alzheimer's disease stages using resting-state fMRI and residual neural networks. J Med Syst 44(2):1–16

Article Google Scholar

28. Raza M, Awais M, Ellahi W, Aslam N, Nguyen HX, Le-Minh H (2019) Diagnosis and monitoring of Alzheimer's patients using classical and deep learning techniques. Expert Syst Appl 136:353–364

Article Google Scholar

29. Ruiz E, Ramirez J, Górriz JM, Casillas J (2018) Alzheimer's disease computer-aided diagnosis: histogram-based analysis of regional MRI volumes for feature selection and classification. J Alzheimers Dis 65(3):819–842

Article Google Scholar

Article Google Scholar

32. Wen J, Thibeau-Sutre E, Diaz-Melo M, Samper-González J, Routier A, Bottani S, Dormont D et al (2020) Convolutional neural networks for classification of Alzheimer's disease: overview and reproducible evaluation. Med Image Anal 63, 101694

33. Yue L, Gong X, Chen K, Mao M, Li J, Nandi AK, Li M (2018) Auto-detection of Alzheimer's disease using deep convolutional neural networks. In: 2018 14th international conference on natural computation, fuzzy systems and knowledge discovery (ICNC-FSKD). IEEE, pp 228–234

Chapter Google Scholar

Data availability statement

Data sharing not applicable to this article as no datasets were generated or analysed during the current study.

Author information

Authors and Affiliations

Department of Computer Science and IT, Dr. Babasaheb Ambedkar Marathwada University,

Correspondence to N. P. Ansingkar.

Additional information

Publisher's note

Springer Nature remains neutral with regard to jurisdictional claims in published maps and institutional affiliations.

Rights and permissions

Reprints and permissions

About this article

Cite this article

Ansingkar, N.P., Patil, R.B. & Deshmukh, P.D. An efficient multi class Alzheimer detection using hybrid equilibrium optimizer with capsule auto encoder. *Multimed Tools Appl* 81, 6539–6570 (2022). https://doi.org/10.1007/s11042-021-11786-z

Received	Revised	Accepted
01 July 2021	23 September 2021	02 December 2021

Published	Issue Date
14 January 2022	February 2022

DOI

Keywords

Pre-processing Segmentation Feature extraction Optimization

Classification Alzheimer detection